AEDC-TR-91-10

C.2

Radiation Model for Flows in High-Pressure Arc Heaters

E. J. Felderman
and
W. N. MacDermott
Calspan Corporation/AEDC Operations

January 1992

Final Report for Period October 1, 1989 to September 30, 1991

ARNOLD ENGINEERING DEVELOPMENT CENTER
ARNOLD AIR FORCE BASE, TENNESSEE
AIR FORCE SYSTEMS COMMAND
UNITED STATES AIR FORCE

NOTICES

When U. S. Government drawings, specifications, or other data are used for any purpose other than a definitely related Government procurement operation, the Government thereby incurs no responsibility nor any obligation whatsoever, and the fact that the Government may have formulated, furnished, or in any way supplied the said drawings, specifications, or other data, is not to be regarded by implication or otherwise, or in any manner licensing the holder or any other person or corporation, or conveying any rights or permission to manufacture, use, or sell any patented invention that may in any way be related thereto.

Qualified users may obtain copies of this report from the Defense Technical Information Center.

References to named commercial products in this report are not to be considered in any sense as an endorsement of the product by the United States Air Force or the Government.

This report has been reviewed by the Office of Public Affairs (PA) and is releasable to the National Technical Information Service (NTIS). At NTIS, it will be available to the general public, including foreign nations.

APPROVAL STATEMENT

This report has been reviewed and approved.

KEVIN T. ZYSK
Propulsion Division
Directorate of Technology
Deputy for Operations

Approved for publication:

FOR THE COMMANDER

KEITH L. KUSHMAN
Director of Technology
Deputy for Operations

REPORT DOCUMENTATION PAGE

Form Approved
OMB No. 0704-0188

1. AGENCY USE ONLY (Leave blank)	2. REPORT DATE	3. REPORT TYPE AND DATES COVERED
	January 1992	Final - Oct. 1, 1989 - Sept. 30, 1991

4. TITLE AND SUBTITLE
Radiation Model for Flows in High-Pressure Arc Heaters

5. FUNDING NUMBERS
PN - DB95VC

6. AUTHOR(S)
Felderman, E. J. and MacDermott, W. N., Calspan Corporation/AEDC Operations

7. PERFORMING ORGANIZATION NAME(S) AND ADDRESS(ES)
Arnold Engineering Development Center/DOF
Air Force Systems Command
Arnold Air Force Base, TN 37389-5000

8. PERFORMING ORGANIZATION REPORT NUMBER

9. SPONSORING/MONITORING AGENCY NAMES(S) AND ADDRESS(ES)
Arnold Engineering Development Center/DOT
Air Force Systems Command
Arnold Air Force Base, TN 37389-5000

10. SPONSORING/MONITORING AGENCY REPORT NUMBER
AEDC-TR-91-10

11. SUPPLEMENTARY NOTES
Available in Defense Technical Information Center (DTIC).

12a. DISTRIBUTION/AVAILABILITY STATEMENT
Approved for public release; distribution is unlimited.

12b. DISTRIBUTION CODE

13. ABSTRACT (Maximum 200 words)

Analytical solutions of the integral equation of energy transport have so facr been limited to a few simple geometries, one of which is the field with cylindrical symmetry - a good match with the geometry of modern high-pressure arc heaters, provided the electric discharge remains on the centerline of the heater. Unfortunately, it is known that the arc column in such devices undergoes substantial excursions from the centerline a large part of the time. To deal with the resulting strong asymmetries in temperature, the radiation transport was modeled using the differential (diffusion) approximation. This results in a partial differential equation which can be solved in multiple dimensions by the same methods that are used to solve the gasdynamic equations. The method has been verified by duplicating the one-dimensional formal integration results.

14. SUBJECT TERMS	15. NUMBER OF PAGES
radiation, arc heaters, heat transfer	54
	16. PRICE CODE

17. SECURITY CLASSIFICATION OF REPORT	18. SECURITY CLASSIFICATION OF THIS PAGE	19. SECURITY CLASSIFICATION OF ABSTRACT	20. LIMITATION OF ABSTRACT
UNCLASSIFIED	UNCLASSIFIED	UNCLASSIFIED	Same as Report

PREFACE

The work reported herein was conducted by the Arnold Engineering Development Center (AEDC), Air Force Systems Command (AFSC), at the request of the AEDC Directorate of Technology (DOT). The Project Manager was Maj. D. C. Hart, AEDC/DOTR. The results were obtained by Calspan Corporation/AEDC Operations, operating contractor for Aerospace Flight Dynamics testing at AEDC. This report contains results obtained under the AEDC Technology Project, Arc Heater Technology (Project No. DB95VC), during the period from October 1, 1989 to September 30, 1991, and the manuscript was submitted for publication on January 2, 1992.

CONTENTS

ILLUSTRATIONS

Figure Page

APPENDIX

1.0 INTRODUCTION

Analysis of gas flows in which there is significant energy transfer by radiation requires a method of analysis of the radiant energy transfer field. Analytical solutions of the integral equation of radiant energy transport have so far been limited to a very few simple geometries, one of which is the field with cylindrical symmetry — a good match with the geometry of modern high-pressure arc heaters, provided the electric discharge remains on the centerline of the heater. Unfortunately, the arc column in such devices undergoes substantial excursions from the centerline a large part of the time. It is therefore desirable to develop analytical methods capable of dealing with strong temperature asymmetries. As part of more general flow-field solutions, development of a means of analysis of nonsymmetric radiation fields is required.

2.0 RADIATIVE ENERGY TRANSFER IN HOT GASES

Analysis of behavior of very hot gases requires the modification of the equations of motion by the addition of a radiant energy transfer term to the conservation of energy. Transport of radiant energy in a region of hot gas is described by the spatial and directional variation of the spectral radiation intensity function, $I_\nu(\bar{r}, \bar{\ell})$. This function is defined as the rate of flow of radiant energy of frequency ν in the direction of the unit vector $\bar{\ell}$ at a point specified by $\bar{r}$, per unit area normal to the direction of propagation, per unit solid angle increment about the direction of propagation, and per unit increment of photon frequency about ν. The spatial variation of I_ν in a given direction is described by the radiative transfer equation (RTE) for a nonscattering gas:

$$\frac{dI_\nu}{dS} = - K_\nu \left[I_\nu - B_\nu\right] \tag{1}$$

where B_ν is the equilibrium (blackbody) intensity, K_ν is an attenuation or absorption coefficient, and S is the distance measured in the direction of propagation.

The "gray gas" approximation is frequently justified; namely, the absorption coefficient is independent of photon frequency, $K_\nu = K$; hence, the intensities can be integrated over all frequencies to become:

$$I = \int_0^\infty I_\nu \, d\nu \text{ and } B \equiv \int_0^\infty B_\nu \, d\nu = \sigma T^4/\pi \tag{2}$$

With this approximation, the RTE has the form:

$$\frac{dI}{dS} = - K \left(I - \frac{\sigma T^4}{\pi}\right) \tag{3}$$

The radiant intensity at any point in any given direction of propagation is obtained by integrating this ordinary differential equation along that direction of propagation from the boundary of the radiating gas to the (observation) point, represented formally by:

$$I(\bar{r}, \bar{\ell}) = I(\tau_B)\, e^{-\tau_B} + \frac{\sigma}{\pi} \int_0^{\tau_B} T^4 e^{-\tau}\, d\tau \qquad (4)$$

where the variable τ is the (dimensionless) optical depth along the inverse specified direction of propagation, referenced to the observation point (see Fig. 1a)

$$\tau = \int_0^S K ds \qquad (5)$$

The two terms on the right in the formal solution, Eq. (4), have the following interpretation. The first term is the radiation intensity in direction of $\bar{\ell}$ at a boundary point lying on the inverse projection of $\bar{\ell}$ through the observation point, attenuated by absorption as measured by the optical thickness between the two points. The second term is the summation of contribution of emission in the direction of $\bar{\ell}$ from all points lying between the boundary and observation points, each elementary contribution attenuated by absorption attributable to the corresponding optical thickness between each point and the observation point.

The radiant energy (heat) flux vector in the radiating gas is given by an integration of the intensity function over all possible directions:

$$\bar{q}^R = \Sigma\, q_i^R \bar{i}_i\ ; \qquad q_i^R = \int_0^{4\pi} I(\bar{r}, \bar{\ell})\, \ell_i\, d\Omega \qquad (6)$$

where ℓ_i is a direction cosine of the unit vector $\bar{\ell}$. The radiant energy transport term required for the energy equation is the divergence of the vector $\bar{q}^R$:

$$\nabla \cdot \bar{q}^R = \frac{\partial q_i^R}{\partial x_i} = \frac{\partial}{\partial x_i} \int_0^{4\pi} I \ell_i\, d\Omega = \int_0^{4\pi} \frac{dI}{dS}\, d\Omega \text{ and,}$$

from Eq. (3),

$$\nabla \cdot \bar{q}^R = -K \left[\int_0^{4\pi} I(\bar{r}, \bar{\ell})\, d\Omega - 4\sigma T^4 \right] \qquad (7)$$

The radiant intensity in both Eqs. (6) and (7) is obtained from the formal solution of the RTE, Eq. (4):

$$q_i^R = \int_0^{4\pi} \left[I(\tau_B) e^{-\tau_B} + \frac{\sigma}{\pi} \int_0^{\tau_B} T^4\, e^{-\tau}\, d\tau \right] \ell_i d\Omega \qquad (8a)$$

$$\nabla \cdot \bar{q}^R = -K \left[\int_0^{4\pi} \left[I(\tau_B) e^{-\tau_B} + \frac{\sigma}{\pi} \int_0^{\tau_B} T^4\, e^{-\tau}\, d\tau \right] d\Omega - 4\sigma T^4 \right] \qquad (8b)$$

Examination of these relations shows that the extreme complexity in calculating $\bar{q}^R$ or $\nabla \cdot \bar{q}^R$ for any but the simplest geometry lies in obtaining integral solutions of the RTE for a very large number of directions of propagation at each point, to provide a well-defined integrand for the $\int_0^{4\pi}$ integrals. (In principle, the RTE must be satisfied in **all** directions in a 4π solid angle at each point). This results from the fact that the radiant intensity is not a vector quantity definable in terms of only three components.

3.0 EXACT ANALYTICAL SOLUTIONS

Clearly, Eq. (8b) forms a very complicated integro-differential equation for the radiant heat addition term in the energy conservation equation. Exact analytical solutions have been limited to very simple cases involving a single independent space variable, either one-dimensional or axisymmetric cases. ("Exact" solution here means that, within the gray gas approximation, Eqs. (8a) and (8b) are satisfied for all directions of propagation at all points of the radiation field).

3.1 ONE-DIMENSIONAL (PLANAR) CASE

The radiant field in a gray gas lying between two plane parallel black walls of infinite extent has been subject to exact analysis (Refs. 1—2). The location between the two plates is defined by the optical thickness function (see Fig. 1b),

$$\eta(x) \equiv \int_0^x K\, dx' \tag{9}$$

with x measured normal to the wall. Note the difference between this function and the optical depth function, Eq. (5), which is evaluated in the direction of propagation. The radiant heat addition term in this case is found to be:

$$\begin{aligned} -\frac{\partial q^R}{\partial x} = 2K\sigma \Bigg[& T_{WL}^4 \int_0^1 e^{-\eta/\ell}\, d\ell + \int_0^{\eta} T^4 \int_0^1 \exp\left(\frac{-(\eta-\eta')}{\ell}\right) \frac{d\ell}{\ell}\, d\eta' \\ & + T_{WR}^4 \int_0^1 \exp\left(-\frac{\eta_{WR}-\eta}{\ell}\right) d\ell \\ & + \int_{\eta}^{\eta_{WR}} T^4 \int_0^1 \exp\left(\frac{-(\eta'-\eta)}{\ell}\right) \frac{d\ell}{\ell}\, d\eta' - 2T^4 \Bigg] \end{aligned} \tag{10}$$

where subscripts R and L refer to right and left walls, η' is a running variable of integration normal to the wall, ℓ is the cosine of the angle between the propagation direction and the normal to the walls, and $T = T(\eta)$. Integrations over ℓ represent the integration of intensity

over all possible directions in a 4π solid angle. These integrals belong to the family of integro-exponential functions defined by:

$$E_n(Z) = \int_0^1 \ell^{n-2} e^{-Z/\ell} \, d\ell \tag{11}$$

which functions have been evaluated and tabulated by various authors (Ref. 3). In terms of these functions, the heat addition term is:

$$-\frac{\partial q^R}{\partial x} = 2K\sigma \left[T_{WL}^4 E_2(\eta) + \int_0^{\eta} T^4 E_1(\eta - \eta') \, d\eta' + T_{WR}^4 E_2(\eta_{WR} - \eta)\right. \tag{12}$$

$$\left. + \int_{\eta}^{\eta_{WR}} T^4 E_1(\eta' - \eta) \, d\eta' - 2T^4\right]$$

The radiant heat flux vector itself is normal to the walls with a magnitude:

$$q^R = 2\sigma \left[T_{WL}^4 E_3(\eta) + \int_0^{\eta} T^4 E_2(\eta - \eta') \, d\eta' - T_{WR}^4 E_3(\eta_{WR} - \eta) - \right.$$
$$\left. \int_{\eta}^{\eta_{WR}} T^4 E_2(\eta' - \eta) \, d\eta'\right] \tag{13}$$

As noted, Eqs. (12) and (13) provide the exact solution of the radiative transfer equation for the plane-wall case, with the gray gas approximation. A family of such solutions for radiative heat flux between two parallel walls is plotted in Fig. 2 for a range of optical thickness from 0.244 to 12.0 and for a linear gas temperature distribution from 25,000 to 5,000°R. This range of optical thickness was obtained by holding the absorption coefficient constant ($K = 24.4\ ft^{-1} = 0.80052\ cm^{-1}$) and allowing wall spacing (Δ), to vary from 0.12 to 6.0 in. Inspection of Eq. (13) shows that zero optical thickness would give a constant heat flux, $q^R = \sigma [T_{WL}{}^4 - T_{WR}{}^4] = 185{,}500\ Btu/ft^2sec$ at all points between the walls. As the optical thickness is increased, the heat flux decreases because of absorption, and a flux maximum is established at some point near the hotter wall.

In a frequently used approximation, the integro-exponentials, Eq. (11), are replaced by simple exponential functions:

$$E_1(Z) \equiv abe^{-bZ},\ E_2(Z) \equiv ae^{-bZ},\ E_3(Z) \equiv \frac{a}{b} e^{-bZ} \tag{14}$$

with $a = 3/4$, $b = 3/2$. The basic goal of an "exact" solution, namely, the satisfaction of the RTE in all possible directions, is not compromised to any substantial degree by use of this approximation. The heat flux expression becomes:

$$q^R = 2\sigma \left[T_{WL}^4 \frac{1}{2} e^{-3/2\eta} + \frac{3}{4} \int_0^{\eta} T^4 e^{-3/2(\eta-\eta')} d\eta' - T_{WR}^4 \frac{1}{2} e^{-3/2(\eta_{WR}-\eta)} \right. \quad (15)$$

$$\left. - \frac{3}{4} \int_{\eta}^{\eta_{WR}} T^4 e^{-3/2(\eta'-\eta)} d\eta' \right]$$

The radiant heat flux between two parallel plane walls obtained from Eq. (15) is compared with the exact values from Eq. (13) for the two extremes of optical thickness, 0.244 and 12.0, in Fig. 3. While the exponential approximation appears to give quite accurate results for both cases, there is no great computational advantage associated with the approximation.

3.2 CYLINDRICALLY SYMMETRIC CASE

Analytical solutions which satisfy the RTE in all possible directions have also been obtained for the case of cylindrically symmetric geometry (Refs. 4—5). These solutions represent the radiation field inside an infinitely long circular cylinder having a black wall and containing a gas with temperature and absorption coefficient profiles which depend on the radial coordinate only. This configuration is a good approximation to the AEDC high-pressure arc heaters. The radiant heat flux profile in this configuration is given by Eq. (24) of Ref. 4, which is similar to, but more complex than Eq. (13) above, and contains exponential integral functions

$$D_n(Z) = \int_0^1 \frac{\ell^{n-1}}{(1+\ell^2)^{1/2}} \exp\left\{-Z/\ell\right\} d\ell \quad (16)$$

which are equivalent to the $E_n(Z)$ family (Eq. 11) appearing in the plane-parallel solution.

The arc heater radiation field was represented by this model in the Aerotherm ARCFLOW program (Ref. 5), except that as in Eq. (14), simple exponential functions were used to approximate the $D_n(Z)$ integral functions:

$$D_2(Z) = \frac{5\pi}{16} e^{-5/4Z} \text{ and } D_3(Z) = \frac{\pi}{4} e^{-5/4Z} \quad (17)$$

The McDonnell-Douglas SWIRLARC program (Ref. 6) contains the same radiation model. Since it satisfies the RTE exactly in all directions, except for the exponential approximation, Eq. (17), it is considered to be the most accurate procedure available for calculation of radiation heat transfer in arc heaters. It provides a standard of comparison for approximate solutions.

4.0 APPROXIMATE SOLUTIONS

The complexity of the integro-differential equation system, Eqs. (8a-b), has limited analytical solutions to cases in which there is a single independent variable of position. Such solutions, however, cannot represent the radiation field associated with nonaxisymmetric temperature distribution such as frequently present in a high-pressure arc heater when the electric discharge is displaced from the constrictor centerline. For this reason, approximate solutions which do not satisfy the RTE in all directions of propagation have been investigated.

4.1 DIFFUSION APPROXIMATION

In one approximate method, the behavior of the radiation field is represented by a system of (only) partial differential equations of radiant heat flux and the space-integrated intensity:

$$\nabla \cdot \bar{q}^R = - K \left[I_o - 4\sigma T^4 \right] \tag{18}$$

$$\nabla I_o = - 3K \bar{q}^R \tag{19}$$

where

$$I_o = \int_0^{4\pi} I (\bar{r}, \bar{\ell}) \, d\Omega \tag{20}$$

This approximation of the radiation field by simple partial differential equations is referred to as the "differential" or "diffusion" approximation (since Eq. (19) has the same form as the molecular diffusion equation, Appendix A, Sec. 3.0). These equations may be developed in several different ways, but are shown in Appendix A to be most appropriately the first approximation to the radiant field expanded as an infinite series of spherical harmonic functions. This series can be made arbitrarily close to an exact solution for any radiation field (Ref. 7).

Extensive application of this approximation in the field of neutron transport theory has demonstrated that an appropriate (and approximate) boundary condition is:

$$\left[I_o + mq^R \right]_{wall} = 4\sigma T_w^4 \tag{21}$$

where the constant m may have values of $\sqrt{3}$ or 2.0 (Appendix A, Sec. 2.0).

4.2 COMPARISON WITH EXACT ANALYTICAL SOLUTIONS

The following comparisons were made with the gas temperature specified, i.e., no coupling between the gas energy equation and the RTE.

4.2.1 Plane-Parallel Walls

The radiation field between two plane-parallel black walls obtained by use of the diffusion approximation, Eqs. (18-19) (partial differential equations only), is compared with an exact solution obtained by solution of the integro-differential system, Eq. (15), in Fig. 4. The radiant heat flux distribution is given by the same gas field conditions as in Fig. 3, a linear temperature distribution from 25,000 to 5,000°R and an absorption coefficient of 24.4 ft^{-1}. The solutions are shown for two extremes of optical thickness, 0.214 and 12.2. The diffusion approximation agrees well with the exact result, especially for the optically thick case. Two values of the boundary condition parameter, m, Eq. (21), were used, the Mark value of $\sqrt{3}$ and the Marshak value of 2.0 (Ref. 7). The Marshak value gives the better agreement.

4.2.2 Axisymmetric

The radiation field for an axisymmetric geometry approximately the scale of the AEDC HEAT-H1 arc heater is shown in Fig. 5. A linear gas temperature varying from 25,000°R at the centerline to 5,000°R at the wall was used as was a constant absorption coefficient of 24.4 ft^{-1}. Exact solutions of Kesten (Ref. 4), Chiba (Ref. 8), and Nicolet (Ref. 5) are compared with the present "diffusion approximation" calculation. Agreement was found to be good, especially at the wall.

5.0 DIFFUSION APPROXIMATION IN TWO DIMENSIONS

To demonstrate the utility of the diffusion approximation for multidimensional fields not amenable to exact analytical solutions, a two-dimensional field in a circular cross section, somewhat representative of the AEDC HEAT-H1 arc heater was solved using Eqs. (18) and (19) and the Marshak value of $m = 2.0$ in the boundary condition, Eq. (21). A gas temperature distribution representative of an arc displaced from the centerline was assumed: 25,000°R peak temperature located at 40 percent of the radius of a 2.4-in.-diam cross section with linear variation from this peak to a uniform wall temperature of 5,000°R. The temperature distribution was thus decoupled from the radiation equation. The absorption coefficient was assumed to have a constant value of 24.4 ft^{-1} independent of the temperature, and the wall was considered black.

5.1 SOLUTION PROCEDURE

A Cartesian coordinate system (x, y) was used to define the circular cross section with a uniformly spaced 20 × 20 grid. Variations in the streamwise direction (z coordinate) were neglected. By eliminating the heat flux from Eqs. (18-19), a single partial differential equation was attained for the space-integrated intensity I_0.

$$\frac{\partial}{\partial x}\left(\frac{1}{K}\frac{\partial I_o}{\partial x}\right) = 3KI_o - \left[12K\sigma T^4 + \frac{\partial}{\partial y}\left(\frac{1}{K}\frac{\partial I_o}{\partial y}\right)\right] \tag{22}$$

The numerical solution of this equation for I_o was carried out in an iterative manner as follows:

a. The y derivative in Eq. (22) is evaluated from the previous iteration; hence, it is grouped with the source term (to start the process the initial iteration is taken as I_o = constant). Equation (22) then becomes only a function of x and is solved with an implicit finite difference routine (Ref. 9) along each grid line of y = constant.

b. The coordinate system is then rotated 90 deg, effectively interchanging the roles of x and y, and the procedure outlined above in (a.) is repeated in an iterative manner.

c. The 90-deg rotations are continued until the solution converges.

The boundary condition, Eq. (21), is applied in a direction normal to the boundary, since it was developed for planar fields in which the heat flux is always normal to the boundaries. By use of Eq. (19), it is recast in terms of the integrated intensity I_o only:

$$I_o - \frac{m}{3K}\frac{dI_o}{dn} = 4\sigma T_w^4 \tag{23}$$

where n is in the direction of the inward normal to the circular boundary. In the numerical solution, this boundary condition is applied at non-nodal points on the boundary by interpolation between grid points. The final step in the solution is to obtain the radiant heat flux distribution from the gradient of I_o, Eq. (19).

5.2 NUMERICAL RESULTS

For an initial demonstration of the method in two dimensions, the symmetric temperature distribution on which Fig. 5 was based was used to calculate a radiation distribution in a 2.4-in.-diam circle. The two-dimensional calculation duplicated the results of the one-dimensional calculation shown in Fig. 5. Hence, as previously noted, the diffusion results agree well with those of Kesten (Ref. 4), and others cited on Fig. 5.

The same procedure was then used to obtain the radiation field for the nonsymmetric temperature distribution with the peak temperature displaced a distance equal to 40 percent

of the radius in the positive y-direction. In this first approximation the gas temperature was assumed to vary linearly between the maximum value and the wall value. The results of these calculations are shown in Figs. 6a-c. The radiant heat flux shown along the Y-axis in Fig. 6a strongly reflects the effects of the asymmetric gas temperature. Most notable is that the radiant flux to the wall nearest the maximum gas temperature (i.e., arc centerline) is over four times higher than on the far wall. It will be shown later that the assumption of constant absorptivity greatly overestimates the magnitude of this effect. The radiant flux along and in the direction of the X axis, (Fig. 6b), is symmetric about the Y-axis (because the gas temperature is symmetric); however, the maximum flux occurs at a larger radius than it does in the axisymmetric case. The radiant flux along a 45-deg line (X = Y) (Fig. 6c) simply shows a blending of the two extremes (Figs. 6a-b). The radiant heat flux at the wall is depicted in Fig. 6d at various positions around the circular cross section. The relationship between the location of the temperature peak and the maximum radiant wall heat flux is readily apparent.

The solution for the two-dimensional demonstration problem provides a high degree of confidence that the "diffusion approximation" can be used in a three-dimensional arc heater code currently being developed since the primary gradients will be in the cross-sectional plane.

6.0 DIFFUSION APPROXIMATION APPLIED TO SWIRLARC CODE

To gain some experience in solving the gas energy equation and the "diffusion approximation" RTE in their respective coupled forms, it was decided to incorporate the "diffusion approximation" into the axisymmetric SWIRLARC code (Ref. 6).

6.1 SOLUTION PROCEDURE

The approximate radiation model represented by Eqs. (18), (19), and (21) was added to the system of equations in the SWIRLARC code, replacing the relations representing the exact analytical solution of the radiative transfer equation. The numerical solution procedure used in SWIRLARC is an explicit marching procedure. To ensure that the solution procedure was adequate for the RTE, an implicit solution procedure with one-half the radial mesh size was used for it. The respective coupling terms between the gas energy equation and the RTE were included. The thermal property curve fits which are built into SWIRLARC (including those for absorption coefficient) were used for all calculations.

6.2 NUMERICAL RESULTS

A pair of solutions was first obtained using the standard SWIRLARC code with both 13 and 25 radial mesh points to determine the influence of mesh size on details of the solution, notwithstanding the fact that previous calculations had shown that overall results are not

sensitive to the radial mesh size. These two calculations were made for the HEAT-H1 geometry at conditions of P_o = 22 atm, H_o = 3,570 Btu/lbm, I = 1,200 amp, and Z = 1.2 m in a 5.08-cm (2-in.)-diam bore. The calculated radiant heat flux and temperature distributions are shown on Fig. 7a. Although the maximum radiant heat flux inside the radiant field is considerably higher for the 13-point mesh, the values at the wall agree within 7 percent. This does not seem to be a significant difference in light of the uncertainties in the absorption coefficient for high-temperature air to be discussed in Sec. 8.0. The effect of mesh size on the radial temperature distribution is almost negligible, except near the centerline of the flow field.

Solutions with the diffusion approximation of radiation in the SWIRLARC code were obtained with a 13-point radial mesh for solving the gas dynamic equations and a 25-point mesh for the radiation equations. The resulting calculated radiant heat flux distribution for the same P_o = 22 atm case (Fig. 7a) was found to fall between the 13-point and 25-point calculation of the standard SWIRLARC code, and the radial temperature distributions were essentially unchanged.

Similar calculations (Fig. 7b) were also made for the case of P_o = 115 atm, H_o = 3,200 Btu/lbm, I = 1,600 amp, and Z = 1.6 m. For this high-pressure condition, differences in calculated radiant heat flux and temperature distributions introduced by the diffusion approximation were even less than for the lower pressure case.

It appears that at least for axisymmetric flow and radiation fields, the diffusion approximation of radiative energy transport can be readily coupled to a gas dynamic calculation and will produce temperature and radiant energy transfer distributions that are reasonably close to those obtained with an exact model of the geometries of the radiation field.

7.0 INTERPRETATION OF EXPERIMENTAL DATA

During a test in the AEDC HEAT-H1 arc heater during FY90, high-speed motion pictures were made through a quartz side window in the constrictor wall. Movies were obtained of the image of a short segment of the arc (defined by a narrow slit) as it moved relative to the centerline reference. A schematic of the HEAT-H1 arc heater showing the general heater configuration and the locations where the window segment was installed is presented in Fig. 8. Data were obtained at 50 and 80 atm with the window located in Modules 2, 5, and 8. Short sections of movie film (16 msec) taken near the downstream end of the heater (i.e., Module 2, where heat-transfer rates are the highest) are shown in Fig. 9. Excursions of the arc image from the centerline reference are presumably the result of (nearly) circular motion of the arc column inside the heater, and the width of the trace is an approximate measure of the diameter of the arc column cross section.

7.1 MEASURED VERSUS CALCULATED HEAT FLUX

Heat flux to the arc heater constrictor wall is plotted versus axial position in Fig. 10a for P_o = 52.4 atm, H_o = 2,700 Btu/lb, and in Fig. 10b for P_o = 82.5 atm, H_o = 3,120 Btu/lb. The experimental data are shown as bars which represent the average heat flux for each of the eight modules, based on measured temperature rise in cooling water. The predicted curves shown were calculated with the SWIRLARC code. Note that the predictions for Modules 7 and 8 are suspect because the arbitrary initial profiles used to start the SWIRLARC code have not yet "washed out," and the drop in heat flux between 1.5 and 1.6 m is caused by the addition of the final increment of air which in reality is added in the electrode region downstream of the constrictor (not modeled in SWIRLARC).

The heat load in the upstream end of the heater is primarily radiative. The radiative load is nearly constant while the convective load increases in the downstream direction as the gas velocity increases. As a check, the radiative component was calculated each of the following three ways with the same result:

1. SWIRLARC code with the integrated radiation model;
2. SWIRLARC code with the differential radiation model, axially symmetric; and
3. Differential, 2-D, uncoupled radiation code using a symmetric gas temperature profile from SWIRLARC.

Overall, there is reasonably good agreement between the measured and predicted wall heat flux.

7.2 EFFECT OF AN OFF-CENTER ARC ON THE WALL HEAT TRANSFER

In the previous section the two-dimensional diffusion radiation code was shown to give results consistent with other predictive methods for symmetrical fields and experimental data averaged over each module. The radiation code was next used to investigate the effect of a fluctuating arc location (shown in Fig. 9) on the local wall heat transfer. The following modifications were made to the 2-D radiation code.

a. The grid was increased to (80 × 80).
b. The pressure and temperature dependence of the absorption coefficient, K, was included.
c. The basic, on-centerline arc temperature profile was taken from SWIRLARC and approximated by four piecewise linear segments.

d. The off-centerline arc temperature profile was obtained by shifting the break points between the linear segments by a proportional amount. This process is illustrated in Fig. 11 for two linear segments.

Radiant heat flux calculations were carried out for arc displacements up to 90 percent of the constrictor radius with reservoir conditions representative of H1 operation at 50 and 80 atm and also for a projected operation at 190 atm. The radiant flux profiles were qualitatively similar to those shown in Fig. 6. The ratios of maximum and minimum wall heat flux (near and far wall) to the symmetric arc value are shown in Fig. 12 as a function of the arc displacement for the reservoir conditions noted. The assumption of constant absorptivity used in the textbook problem of Fig. 6 ($K = 24.4\ ft^{-1}$, for 100 atm, 25,000°R) greatly exaggerates the effect of the arc displacement. However, linear fits to the calculated data indicate a 50-percent increase in the near-wall radiant heat flux as the arc approaches the wall at 195 atm. The decrease in the far-wall radiant heat flux is of the same order as the increase at the near wall.

7.3 WALL HEAT-TRANSFER ANALYSIS WITH UNSTEADY BOUNDARY CONDITIONS

A one-dimensional, unsteady numerical model for conduction heat transfer through the 0.080-in. arc heater constrictor wall was developed. The water-side wall temperature was taken as a constant 650°F. This is approximately 100°F above the saturation temperature at 1,000 psia (cooling system pressure) and represents a practical limit on the water-side wall temperature to avoid burnout. This assumption will eventually be improved with the results of a boiling heat-transfer experiment currently underway at AEDC. The unsteady air-side boundary condition is formulated by first assuming that the arc location (Fig. 9) can be represented by a linear oscillation, a fairly poor assumption since the path is probably three-dimensional. For simplicity, the arc position is approximated by a sine wave with period and amplitude matched to the film record (Fig. 9). The instantaneous location of the arc is then used with the results shown in Fig. 12 to determine the radiant wall heat transfer. Finally, the convective component is added to the radiative component to obtain the total heat transfer which serves as the air-side boundary condition for the conduction calculation.

Results of a calculation for a case of 80 atm and 3,120 Btu/lbm are shown in Fig. 13a for a period of 0.001 sec and an amplitude of 90 percent of the constrictor radius. This is a typical value of the period (Fig. 9) and a maximum value of the amplitude. The frequency is sufficiently high so that the water-side heat flux is not affected and the air-side wall temperature rises only a few degrees. The possibility of the arc remaining near the wall for an extended period of time was investigated by using a period of 0.1 sec. The results shown in Fig. 13b show significant rises in both the air-side wall temperature and the water-side

heat-transfer rate. However, the maximum heat flux of 4,000 Btu/ft^2 sec at 80 atm is sufficiently low that wall failure is unlikely, even if the arc remains close to the wall for an indefinite period.

A case at 195 atm, 3,520 Btu/lbm was also investigated. A period of 0.001 sec (taken from the 50- and 80-atm case) and an amplitude of 90 percent of the constrictor radius was used to obtain the results shown in Fig. 14a. Again, the frequency of the arc fluctuation is sufficiently high so that the water-side of the constrictor wall does not respond. The air-side wall temperature responds only slightly, rising about 30°F. The case of the arc remaining near the wall for an extended period was also investigated using a period of 0.1 sec. The results shown in Fig. 14b show significant rises in both the water-side heat transfer and the air-side wall temperature. The wall temperature rises to 1,830°F, which is still below the melting point. The water-side heat-transfer rate peaks at 10,600 Btu/ft^2 sec, which is near the value at which burnout is thought to occur. A response time of sorts may be obtained by looking at the phase shift in Fig. 14a. For the air-side wall temperature this is 0.0088 sec, and 0.015 sec for the water-side heat transfer.

Finally, the temperature profiles through the copper wall at the maximum wall temperature are shown in Fig. 15. If the arc remains on the geometric centerline, the profile is linear. For the low-frequency fluctuation (λ = 0.1 sec) the deviation from linearity is imperceptible, while for the high-frequency fluctuation (λ = 0.001 sec) the nonlinearity begins to show up. The tensile strength of copper for the λ = 0.1 sec case is also plotted in Fig. 15. Although melting has not occurred, the strength of the wall on the air side is quite low.

8.0 RADIATION PROPERTIES OF HIGH-TEMPERATURE AIR

8.1 TWO-BAND MODEL

An attempt was made to resolve the differences in presentation of radiative properties of high-temperature air in a number of references. In Ref. 5, air was characterized as having two gray emission bands, a low-energy band with 0 - 10.5 ev photon energy and a high-energy band with 10.5 - 100 ev photon energy.

Between 2,000 and 30,000°K the low-band absorption coefficients are $K_L = 10^{-5}$ to 4×10^{-1} cm^{-1} and the high-band absorption coefficients are K_H = 1.0 to 1×10^4 cm^{-1}. Although the absorption coefficients are much larger for the high-energy band, the fraction of total blackbody intensity is also very small for this band, <1 percent for temperatures up to 11,000°K. It is therefore possible, under certain conditions, to obtain a good approximation to total radiant intensity using only the low-band absorption coefficient, K_L,

$$I_{IND} = B_T \left(1 - e^{-K_L X}\right) = \frac{\sigma T^4}{\pi} \left(1 - e^{-K_L X}\right) \tag{24}$$

The error made in use of this relation may be assessed by evaluating the ratio:

$$\frac{I_{TOTAL}}{I_{IND}} = \frac{I_L + I_H}{I_{IND}} = \frac{B_L\left(1 - e^{-K_L X}\right) + B_H \left(1 - e^{-K_H X}\right)}{B_T \left(1 - e^{-K_L X}\right)}$$

$$= W_L + W_H \frac{\left(1 - e^{-K_H X}\right)}{\left(1 - e^{-K_L X}\right)} = 1 + W_H \left[\frac{\left(1 - e^{-K_H X}\right)}{\left(1 - e^{-K_L X}\right)} - 1\right] \tag{25}$$

where B_L, B_H are blackbody intensities for the two bands and W_L, W_H are blackbody band-weight factors.

A plot of this ratio is given in Fig. 16 for pressures of 1, 10, 60, and 100 atm, at 1-cm depth of gas and for 0.5 and 2 cm at 10 atm. The emission from air is clearly dominated by the low-energy band for sufficiently high pressures and temperatures less than 15,000 K. The low-band absorption coefficient may be used with good accuracy at $T \leq 12{,}000$ K, $P \geq 60$ atm, and $X \geq 1$ cm, all of which conditions prevail in the high-pressure AEDC arc heaters under normal operating conditions. For pressures of the order of 10 atm and below, however, the errors can become quite large, $\geq$ 100 percent.

8.2 ABSORPTION COEFFICIENT DATA

Radiation properties of high-temperature air are available in a large number of references. A comparison is complicated because of the diverse forms in which the data are presented and also because the thermodynamic states are generally not matched. Integrated hemispheric emission coefficients are given in Refs. 10 - 12, spectral and integrated steradiance in Refs. 13 - 14, and integrated Planck absorption coefficients in Refs. 5 and 11. Most of these references rely on data from precedent original references. In some cases, the emission data are broken down by individual radiating species in the air. For comparison of these data, all were converted to total (integrated) absorption coefficient, interpolated in some cases to match specific thermodynamic states. The absorption coefficient at 1-atm density and temperature from 2,000 to 13,000 K is given in Fig. 17a, from data obtained in the cited references. On Fig. 17b, the absorption coefficient is given as a function of density at T = 6,000 K. The low-band coefficients of Nicolet (Ref. 5), which are also used in the SWIRLARC program, (Ref. 6), agree with data from other sources within a factor of 2.0 to 3.0.

9.0 CONCLUSIONS

Computational exercises have been used to determine whether or not a simplified radiation model (diffusion approximation) can be used for the calculation of high-temperature gas flows in which the radiation fields are not sufficiently symmetric to be amenable to exact analytical solution of the radiative transfer equation. Comparisons of radiation fields calculated exactly and with various approximations were made for simple configurations for which analytical solutions are available. Also, simple axially symmetric flows of hot gases were successfully calculated using approximate radiation field equations coupled to the gas dynamic conservation equations.

1. Based on these results, there appears to be a reasonable basis for applying the diffusion approximation of radiation in flow calculations in which the temperature and radiation fields are nonsymmetrical, such as in an electric arc heater with the discharge displaced from the centerline.

2. Total wall heat-transfer rates measured in the constrictor of the AEDC-H1 arc heater at 50 - 80 atm pressure and 2,700 - 3,100 Btu/lbm enthalpy agreed quite well with predictions made by the SWIRLARC computer program. The radiant flux dominates at the upstream end of the constrictor.

3. An unsteady heat-transfer analysis of the arc heater constrictor walls revealed that the observed fluctuations in arc position were of sufficiently high frequency that the walls will not respond to the fluctuating heat input.

REFERENCES

1. Anderson, J. D., Jr. *Hypersonic and High Temperature Gas Dynamics.* McGraw-Hill, 1989.

2. Vincenti, W. G. and Kruger, C. H., Jr. *Introduction to Physical Gas Dynamics.* John Wiley & Sons, 1965.

3. Kourganoff, V. *Basic Methods in Transfer Problems (Radiative Equilibrium and Neutron Diffusion).* Dover Press, 1963.

4. Kesten, A. S. "Radiant Heat Flux Distribution in a Cylindrically Symmetric Nonisothermal Gas with Temperature Dependent Absorption Coefficient." *Journal of Quantitative Spectroscopic and Radiative Transfer*, Vol. 8, 1963, pp. 419-434.

5. Nicolet, W. E., et al. "Analytical and Design Study for a High-Pressure, High-Enthalpy Constricted Arc Heater." AEDC-TR-75-47 (AD-A012551), July 1975.

6. Shaeffer, J. F. "SWIRL ARC: A Model for Swirling, Turbulent, Radiative Arc Heater Flowfields." AIAA Paper No. 78-68 (1978).

7. Cheng, P. "Study of the Flow of a Radiating Gas by a Differential Approximation." Ph.D. Dissertation, Stanford University, 1965 (available from University Microfilms, Ann Arbor, MI).

8. Chiba, Z. "The Study of Heat Transfer with Radiation to Gases in Turbulent Flow Within Tubes." Ph.D. Thesis in Engineering, University of California, Berkeley, September 1972.

9. Patankar, S. V. "Heat and Mass Transfer in Turbulent Boundary Layers." Ph.D. Thesis, Imperial College of Science and Technology, University of London, June 1967.

10. Yos, J. M. "Transport Properties of Nitrogen, Hydrogen, and Air to 30,000 K." Technical Memorandum RAD-TM-63-7, Research and Advanced Development Division, Avco Corporation, Wilmington, MA, March 22, 1963.

11. Penner, S. S. and Olfe, D. B. *Radiation and Reentry*. Academic Press, New York, 1968.

12. Clarke, J. F. and McChesney, M. *The Dynamics of Real Gases*. Butterworths, Washington, DC, 1964.

13. Martin, J. J. *Atmospheric Reentry* (An Introduction to its Science and Engineering). Prentice-Hall, Inc., Englewood Cliffs, NJ, 1966.

14. Zel'dovich, Y. B. and Raizer, Y. P. *Physics of Shock Waves and High Temperature Hydrodynamic Phenomena*. Academic Press, New York, 1966.

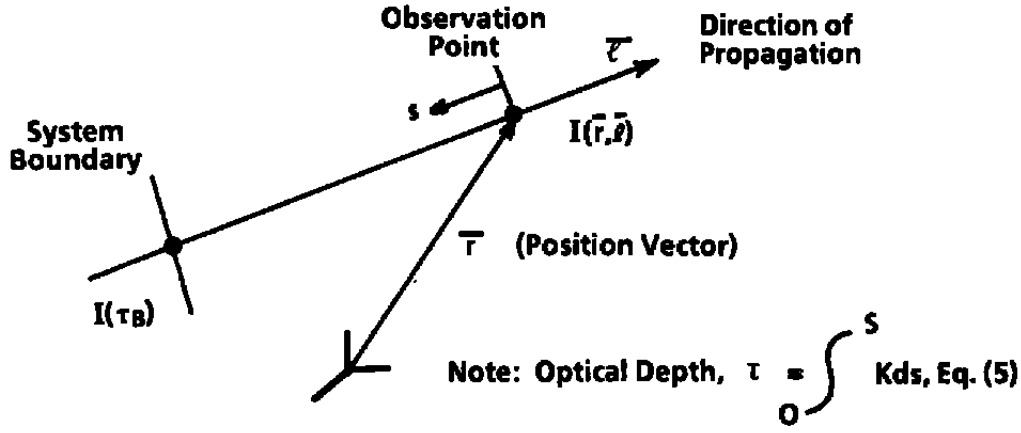

a. Radiant intensity in an emitting and absorbing gas

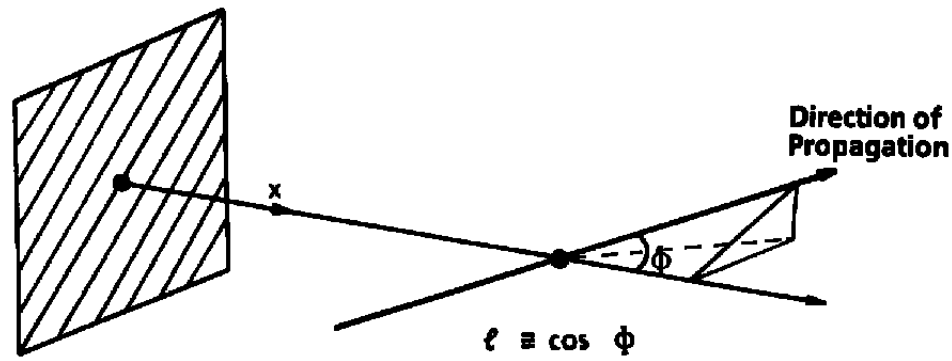

Optical Thickness, $\eta(x) = \int_0^x K dx'$, Eq. (9)

b. One-dimensional case (radiant field between two parallel, infinite black walls)

Figure 1. Geometry considerations for radiant energy transfer in an emitting and absorbing gas.

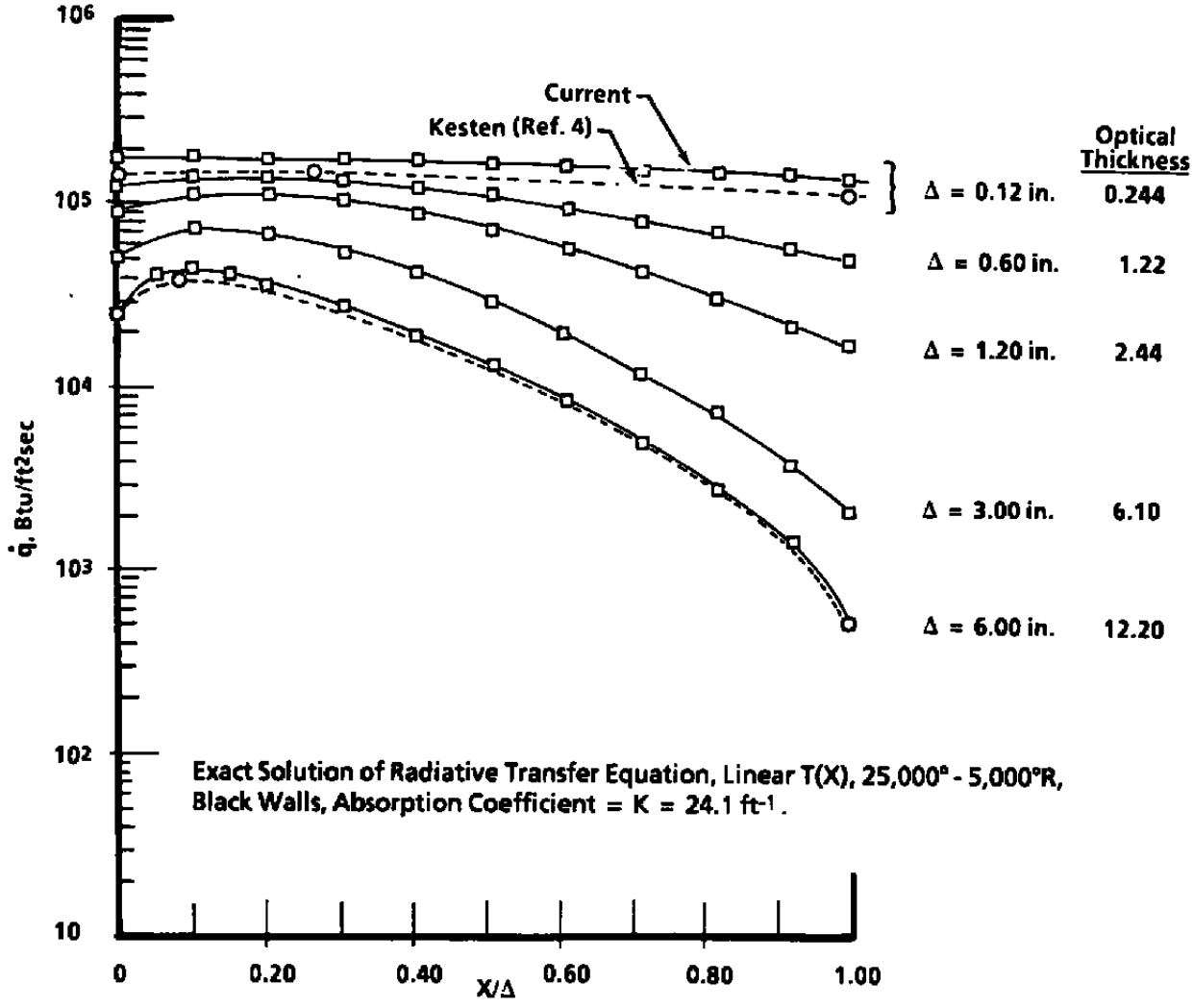

Figure 2. Radiation heat flux between plane walls — optical thickness effects.

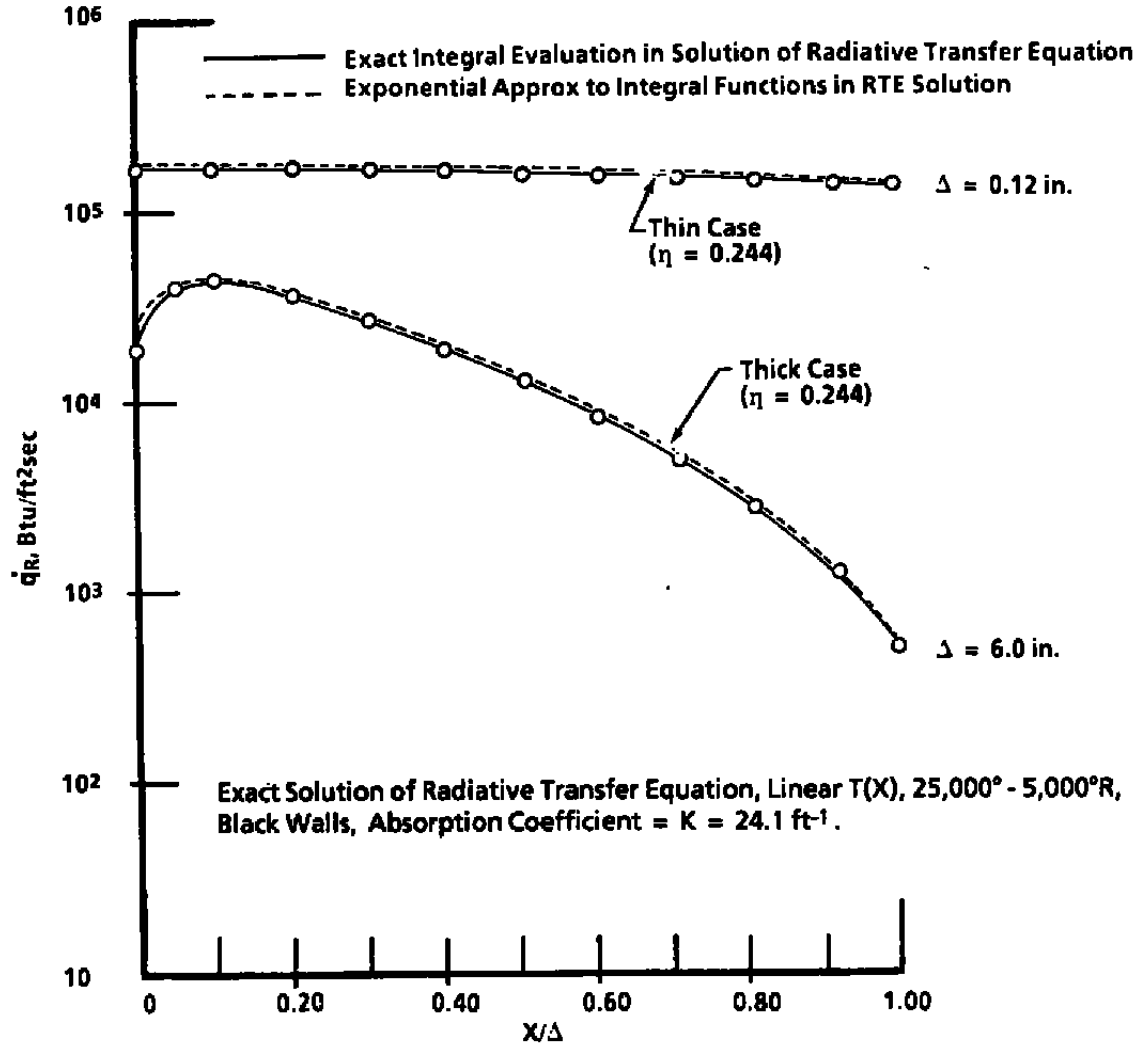

Figure 3. Radiation heat flux between plane walls — exponential approximation compared with exact solution.

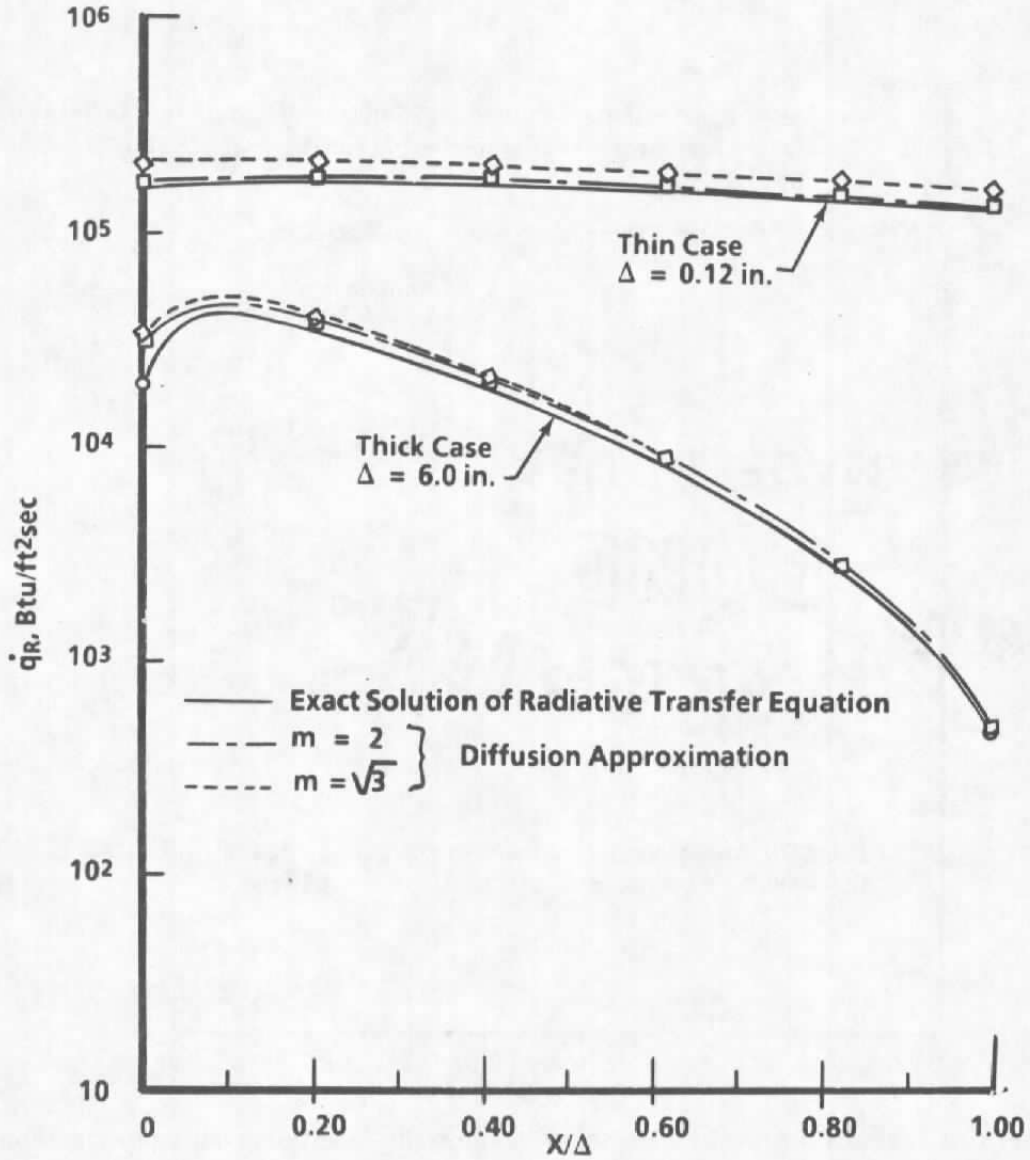

Figure 4. Radiation heat flux between plane walls — diffusion approximation compared with exact solution, linear T(X), 25,000 — 5,000°R, black walls, absorption coefficient = 24.4 ft^{-1}.

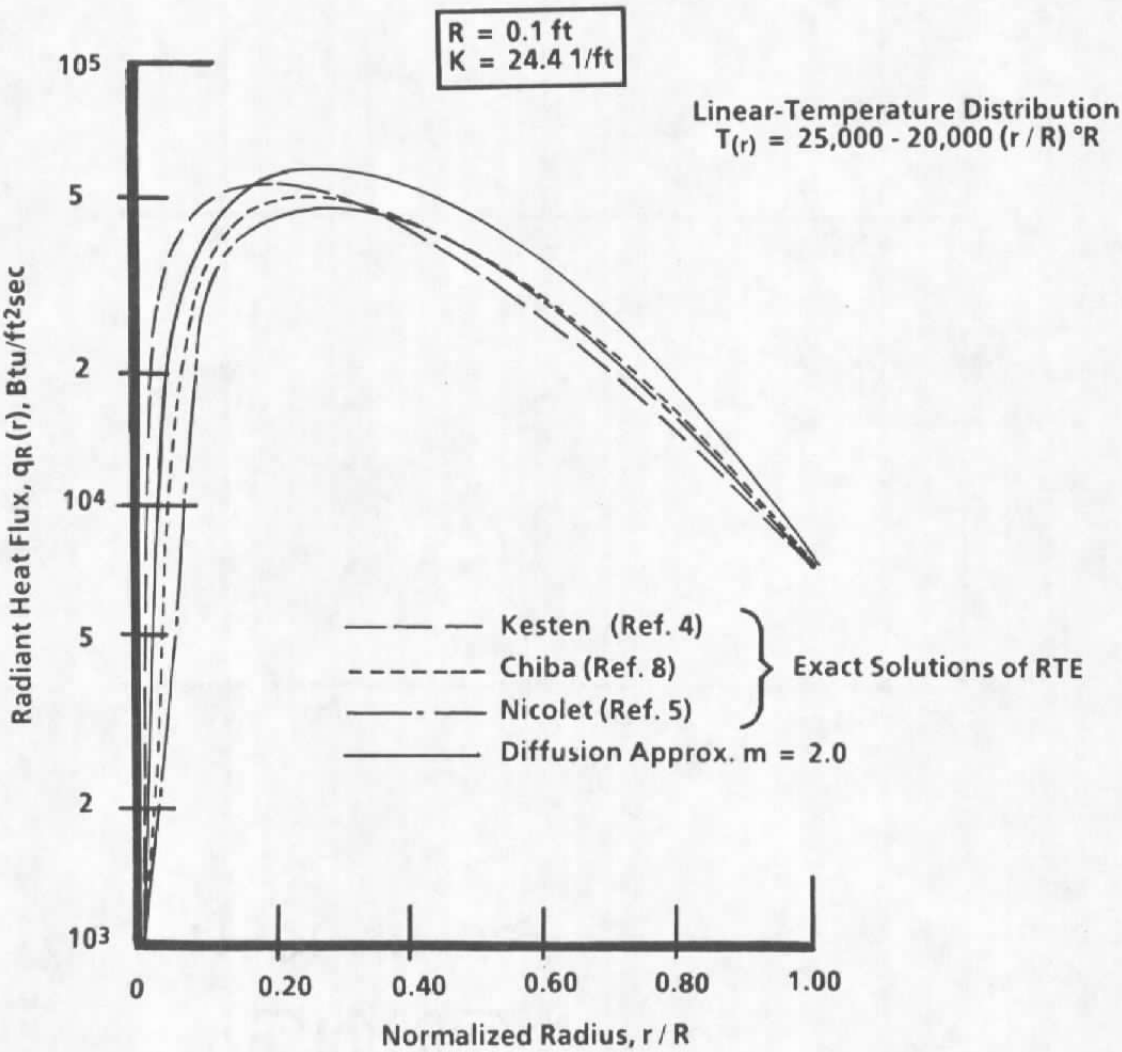

Figure 5. Radiation flux in long circular cylinder — comparison of diffusion approximation with exact solutions.

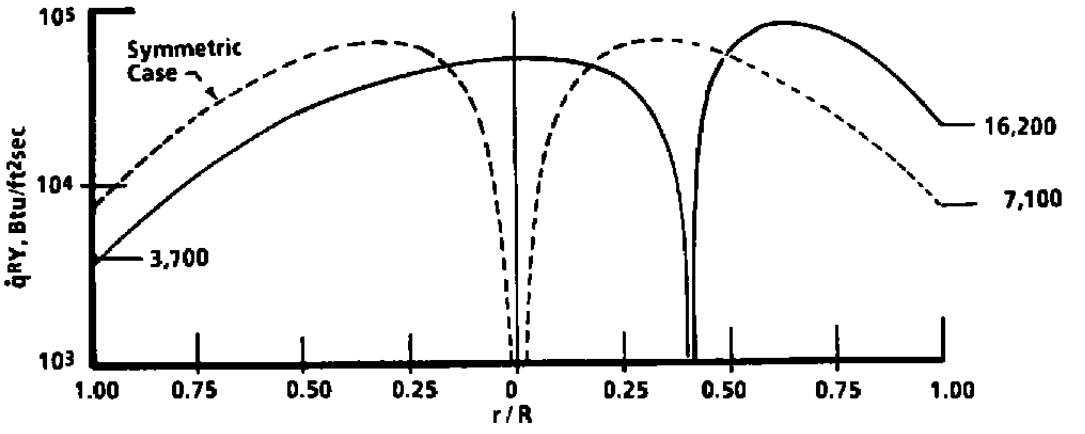

a. $\dot{q}_Y^R$ along Y-axis

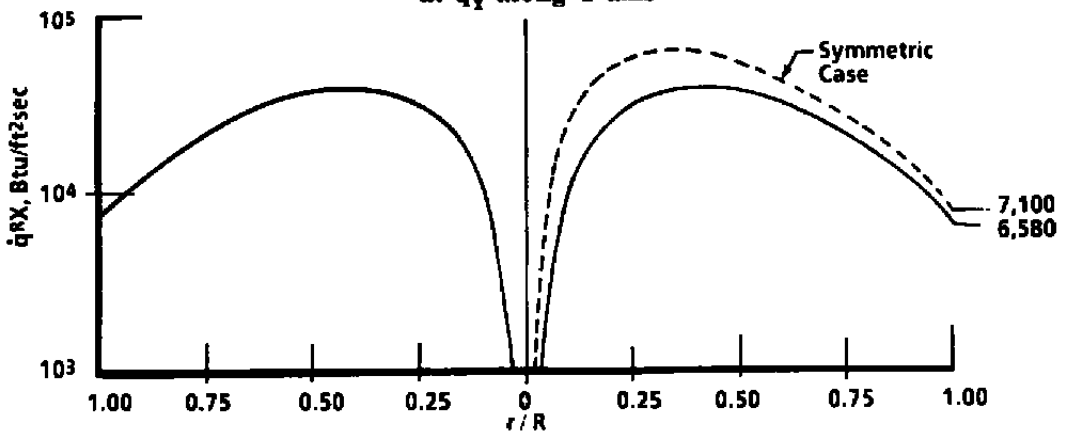

b. $\dot{q}_X^R$ along X-axis

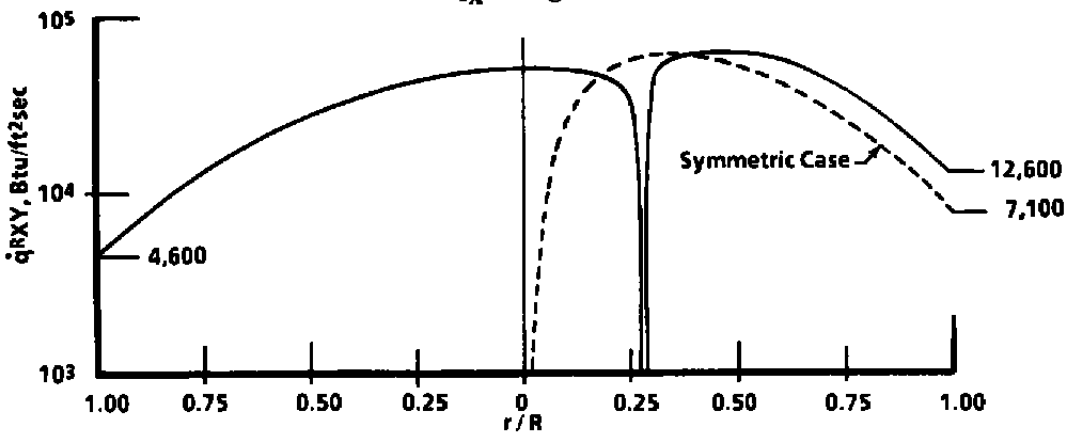

c. $\dot{q}_{XY}^R$ along X = Y diagonal

Figure 6. Radiation heat flux distributions in long circular cylinder with asymmetric temperature distribution, temperature peak at r/R = 0.40, R = 1.2 in.

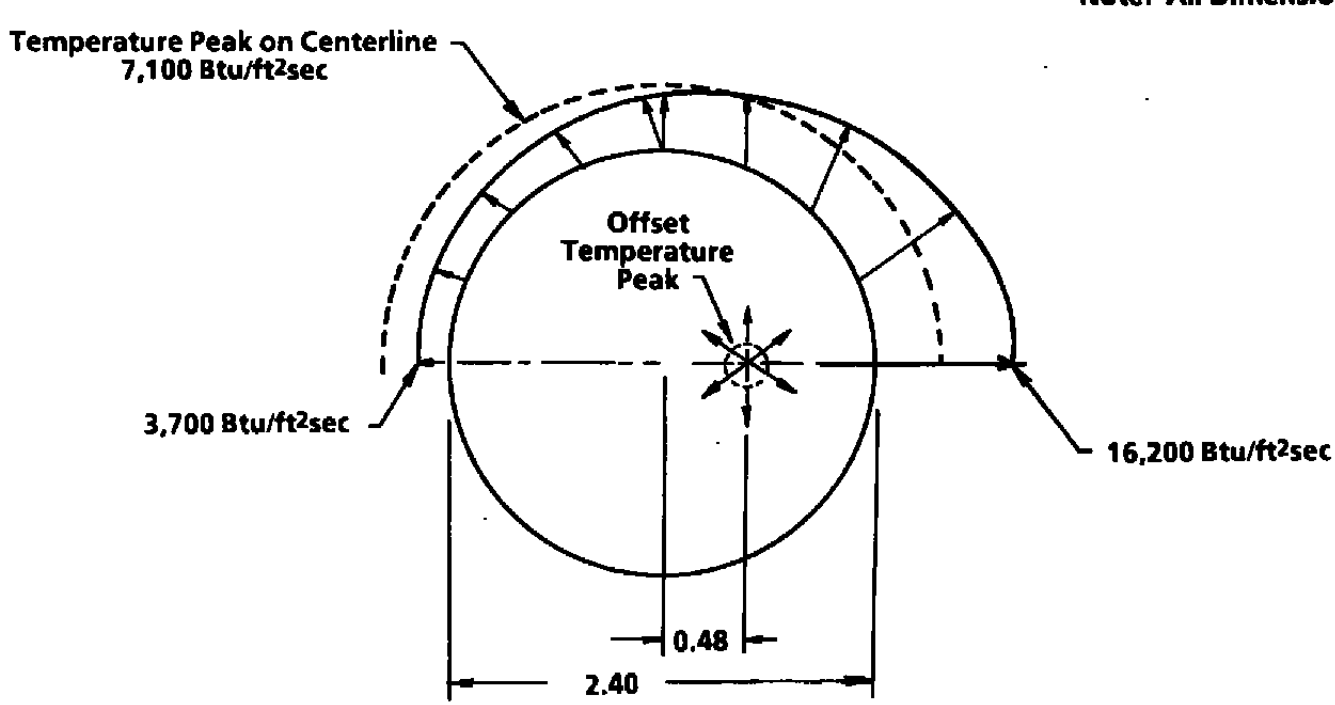

d. Distribution of radiant heat flux at with wall asymmetric temperature distribution: 25,000°R at r/R = 0.4, T_{wall} = 5,000°R, linear, absorption coefficient = 24.4 ft^{-1}.

Figure 6. Concluded.

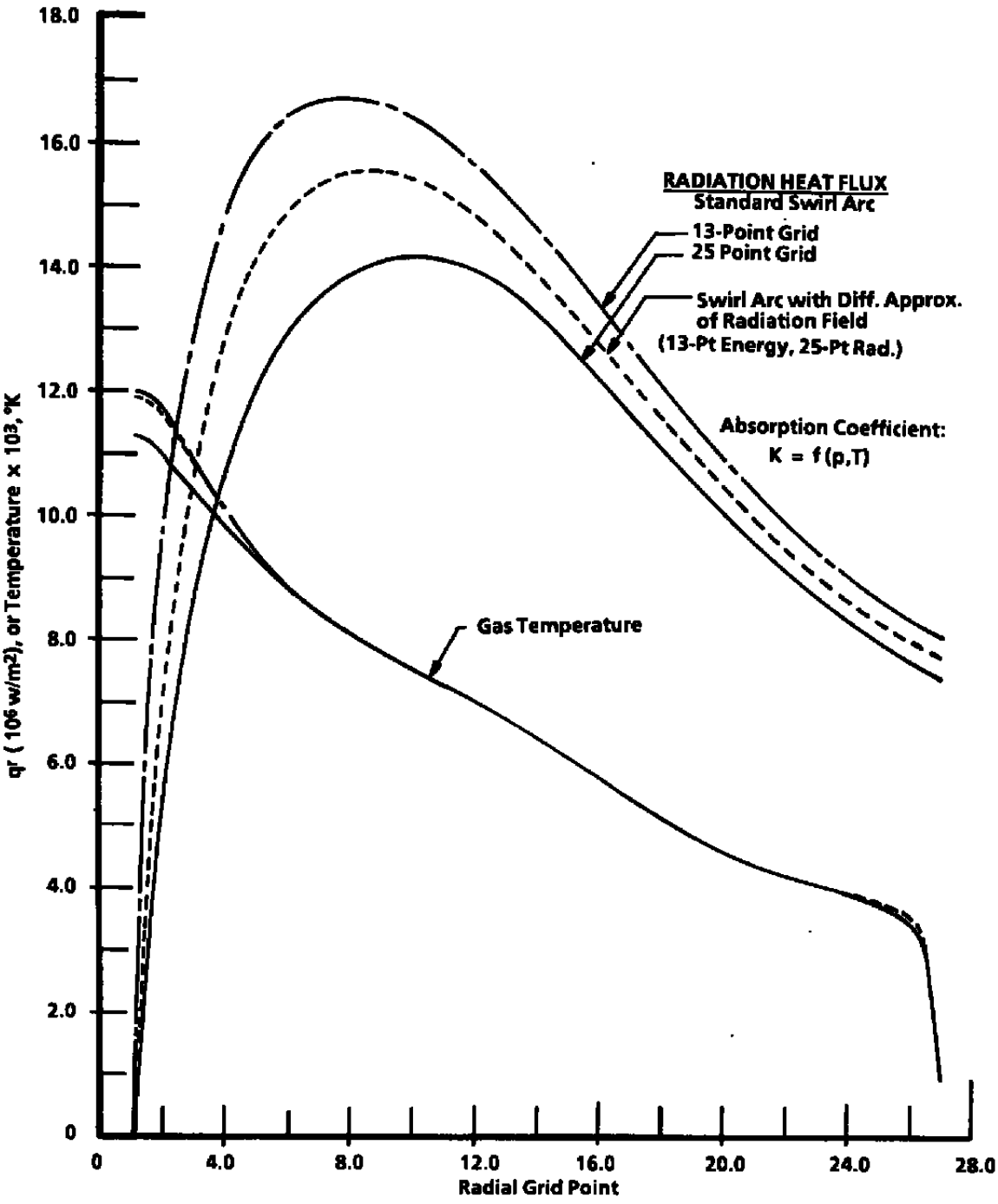

a. P_o = 22 atm, H_o = 3,570 Btu/lbm, I = 1,200 amps, Z = 1.2 m, d = 5.08 cm

Figure 7. Temperature and radiant heat flux distribution in SWIRLARC solutions.

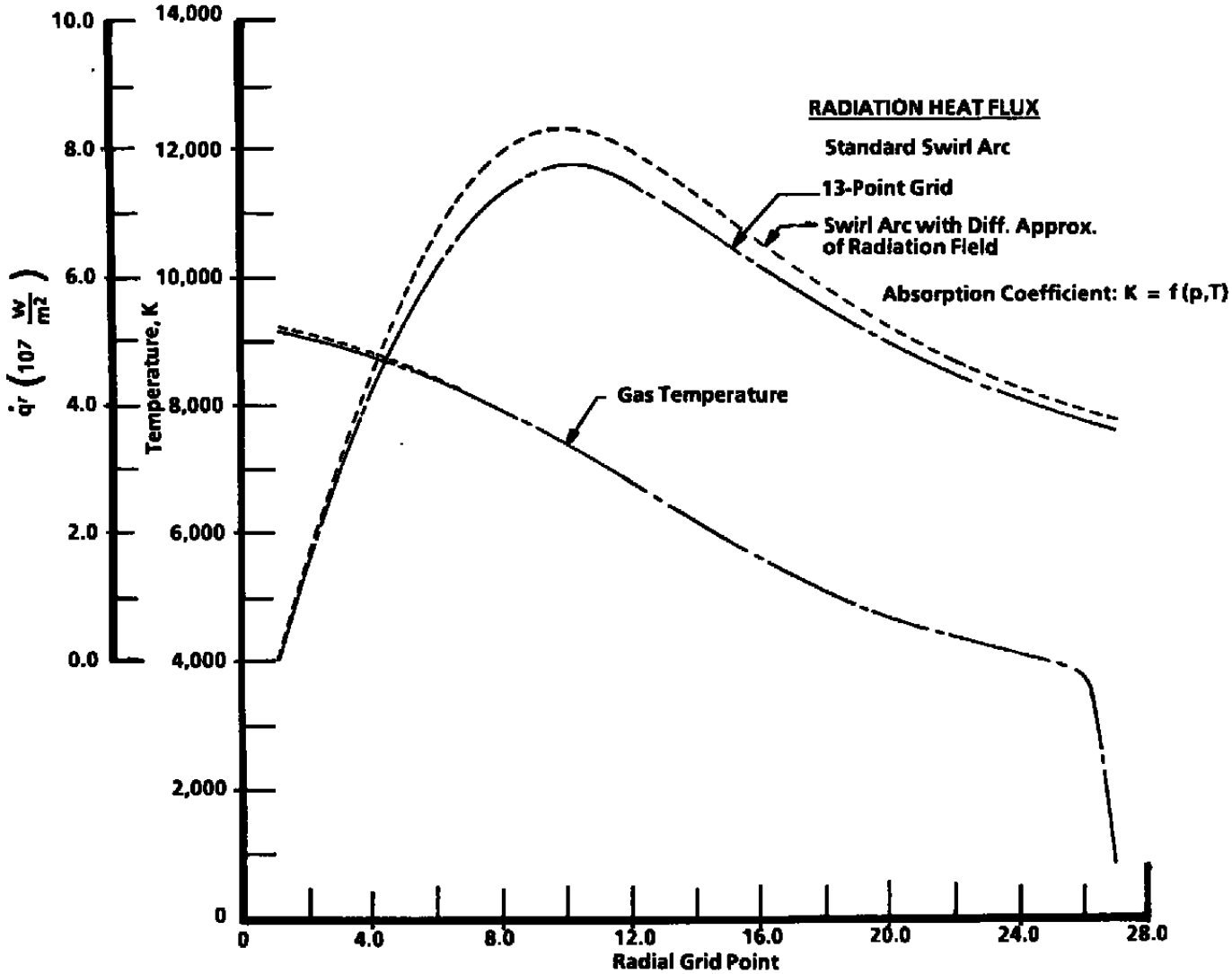

b. P_o = 115 atm, H_o = 3,200 Btu/lbm, I = 1,600 amps, Z = 1.6 m, d = 5.08 cm

Figure 7. Concluded.

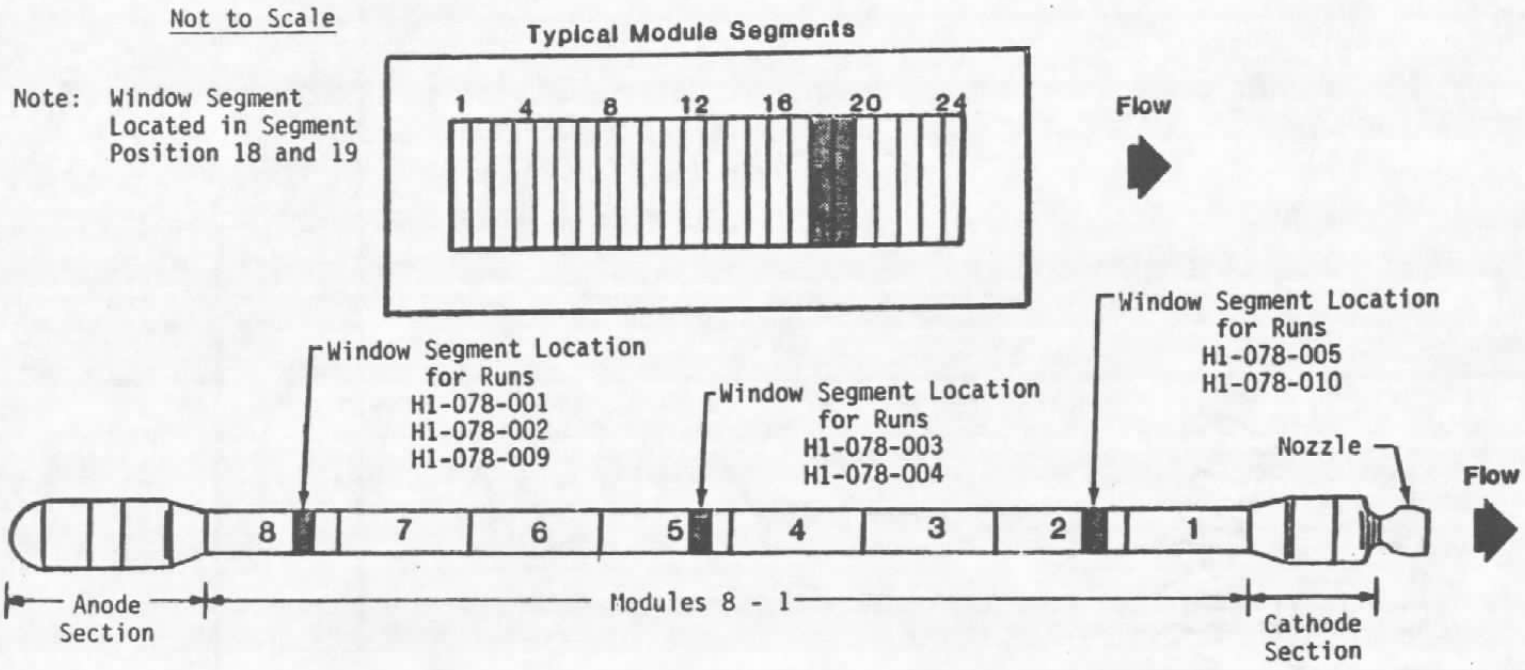

Figure 8. Window segment locations — HEAT-H1 arc heater.

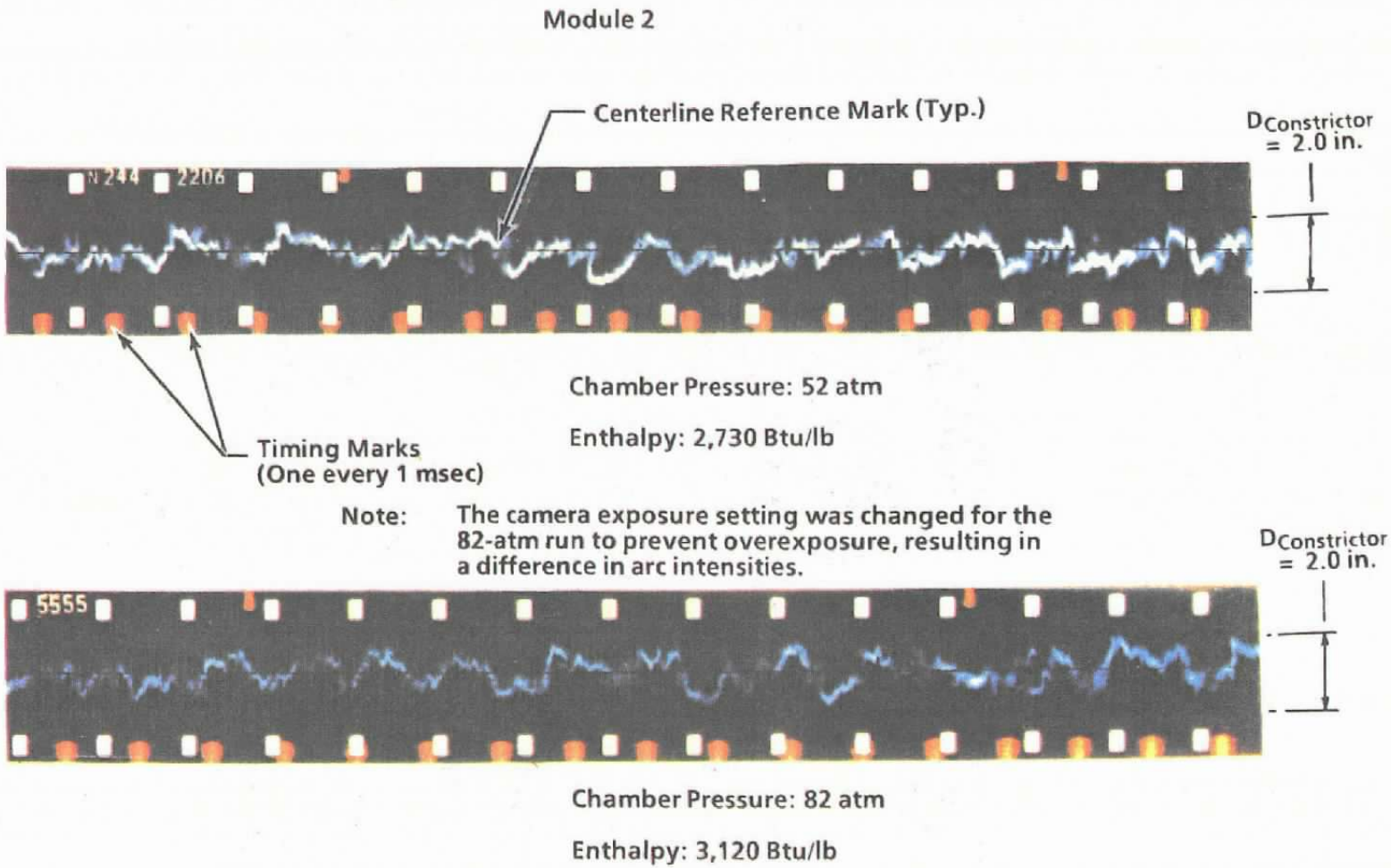

Figure 9. Arc visualization at two different chamber pressures.

Run No.	P_o, atm	H_o, Btu/lbm	m, lbm/sec	Arc Current, amps
H1-078-003	52.7	2,660	2.85	736
H1-078-004	52.4	2,700	2.82	739
H1-078-005	52.5	2,730	2.81	748
H1-078-009	52.4	2,740	2.81	745

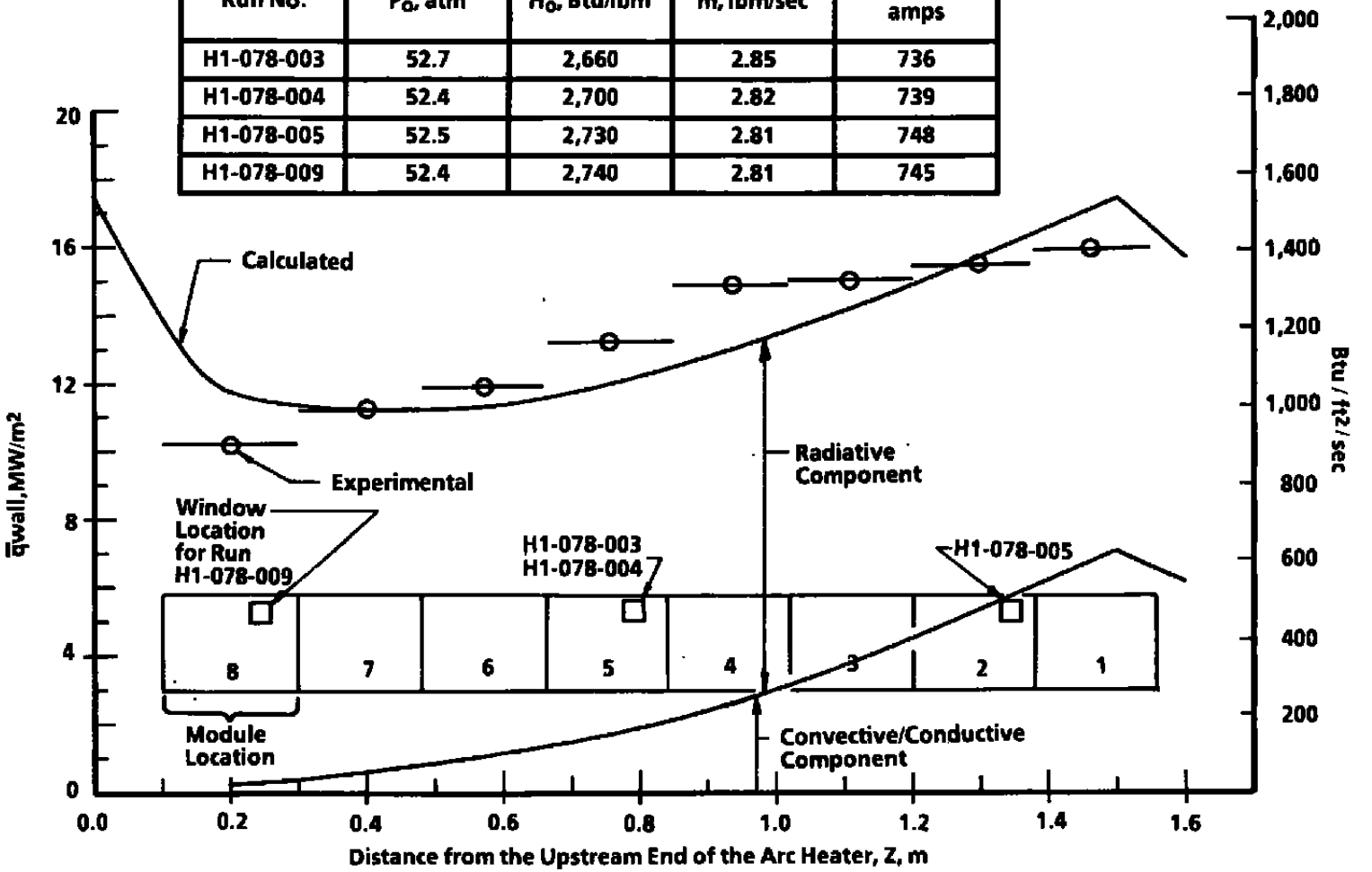

a. 52.5-atm runs

Figure 10. Heat flux measurements in the HEAT-H1 arc heater and comparison with SWIRLARC predictions.

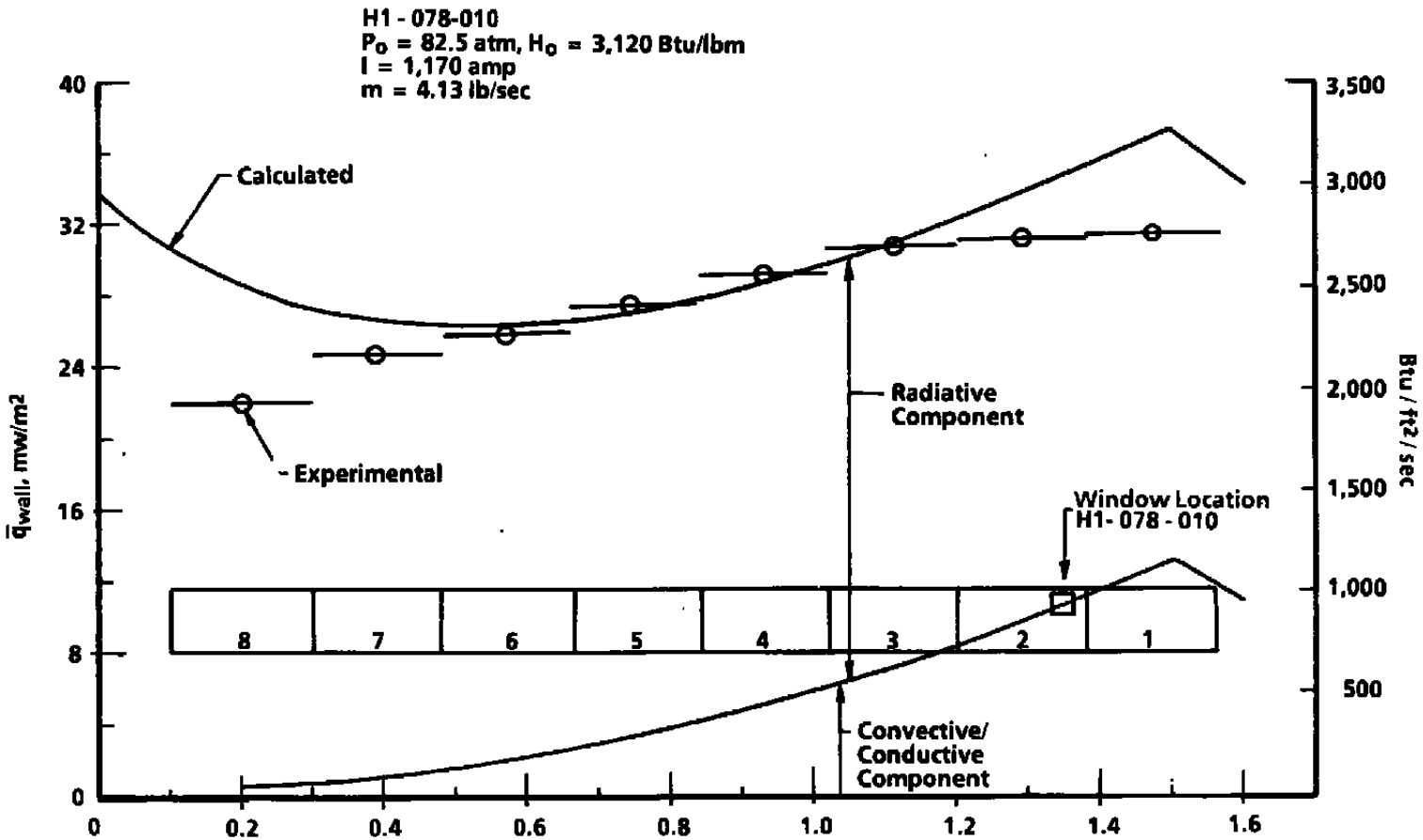

b. 82.5-atm run

Figure 10. Concluded.

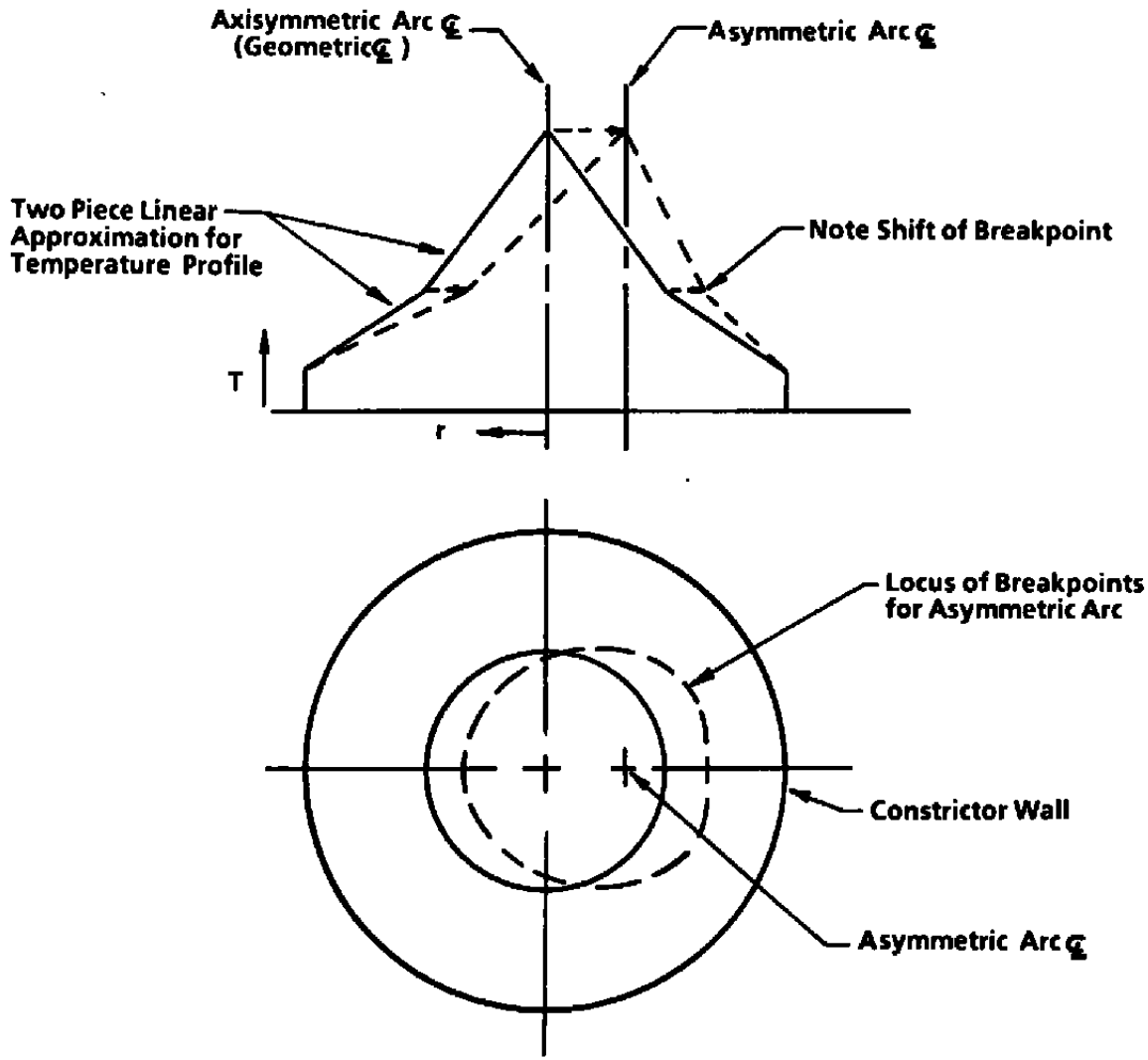

Figure 11. Postulated gas temperature distribution resulting from an off-centerline arc location.

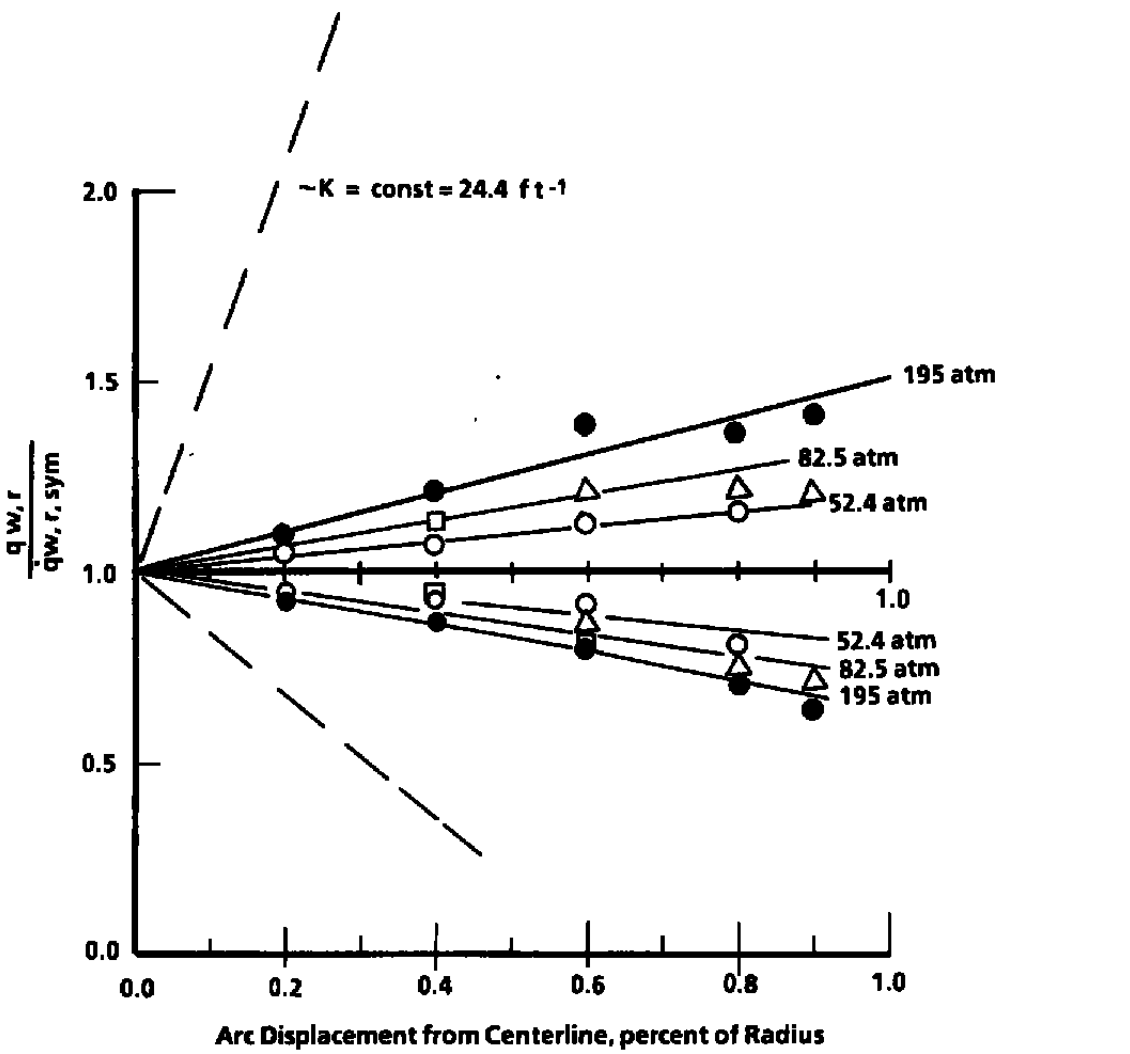

Figure 12. Radiant wall heat flux modification due to off-centerline arc location.

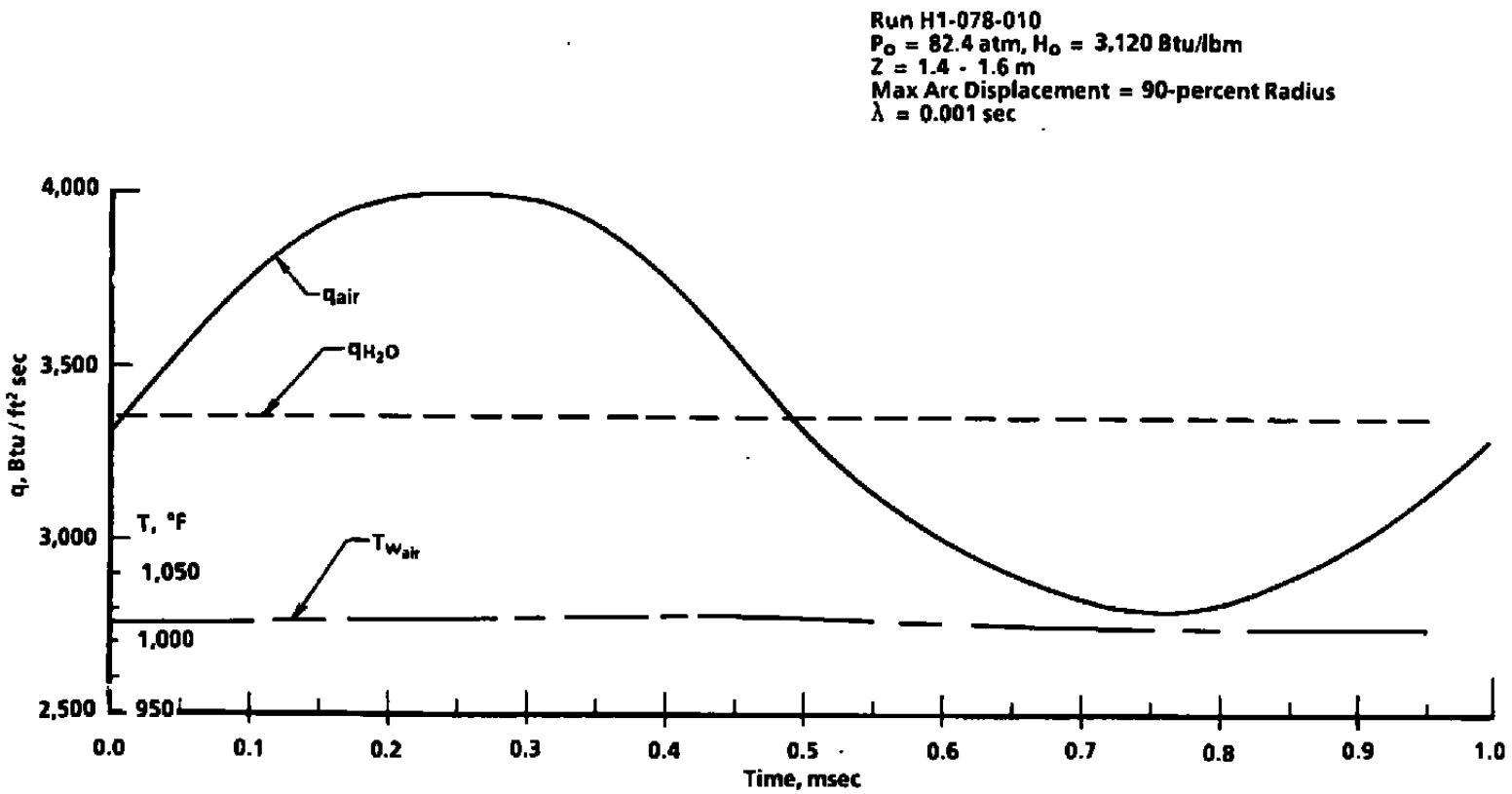

a. Period, λ = 0.001 sec

Figure 13. Predicted constrictor wall response to periodic thermal loading, 82.4 atm, 3,120 Btu/lbm.

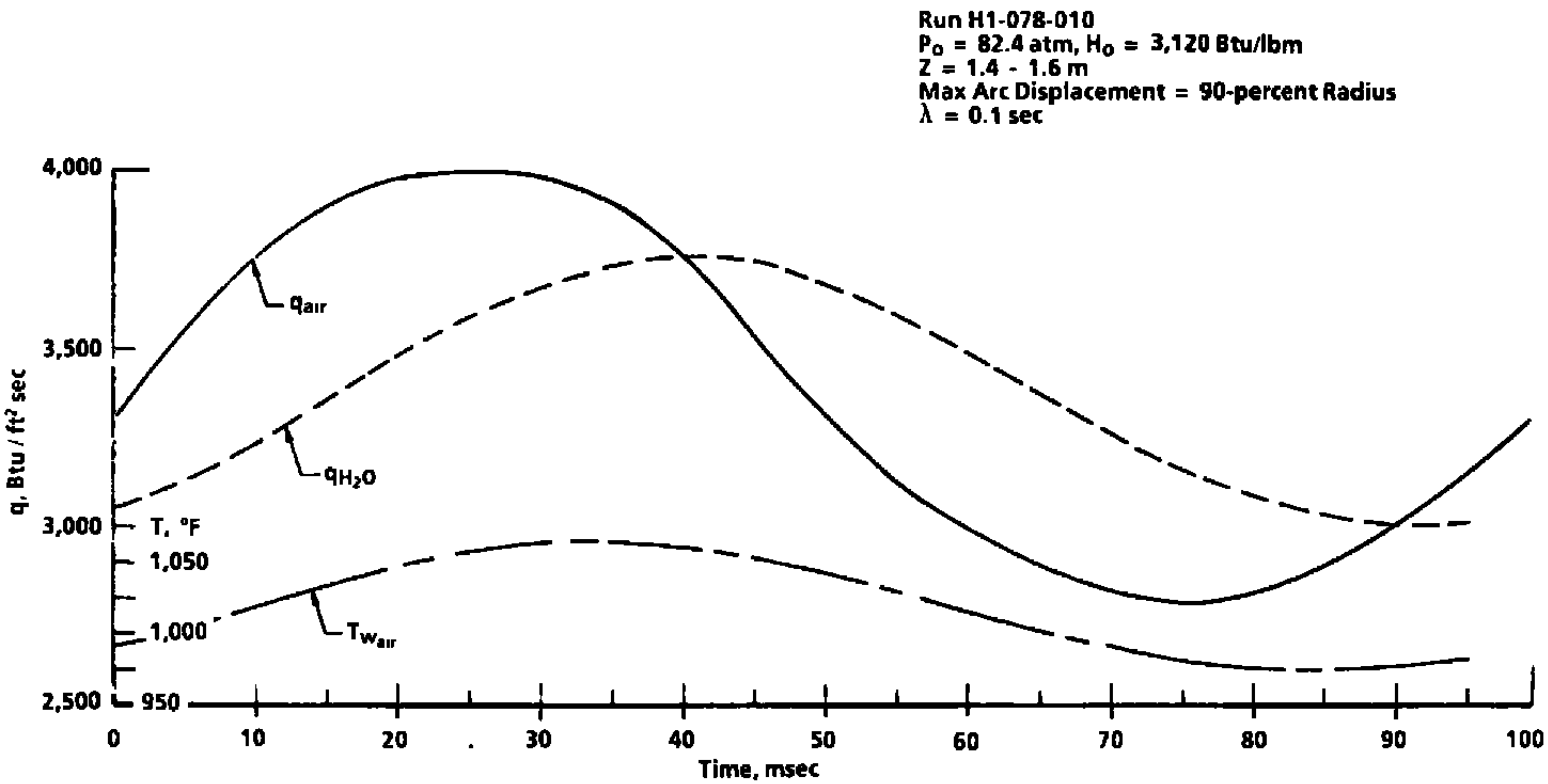

b. Period, λ = 0.1 sec

Figure 13. Concluded.

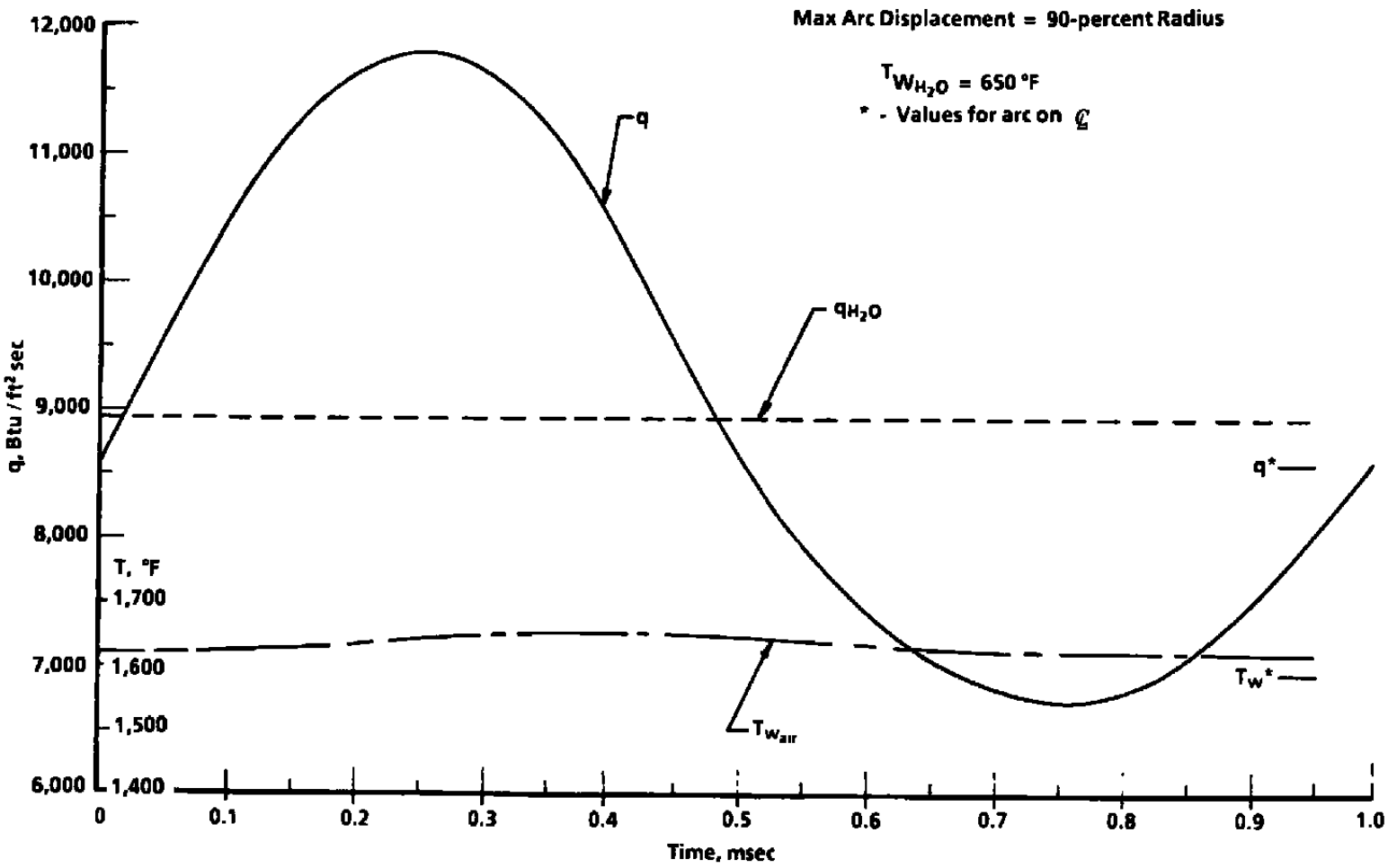

a. Period, λ = 0.001 sec

Figure 14. Predicted constrictor wall response to periodic thermal loading, 195 atm, 3,520 Btu/lbm.

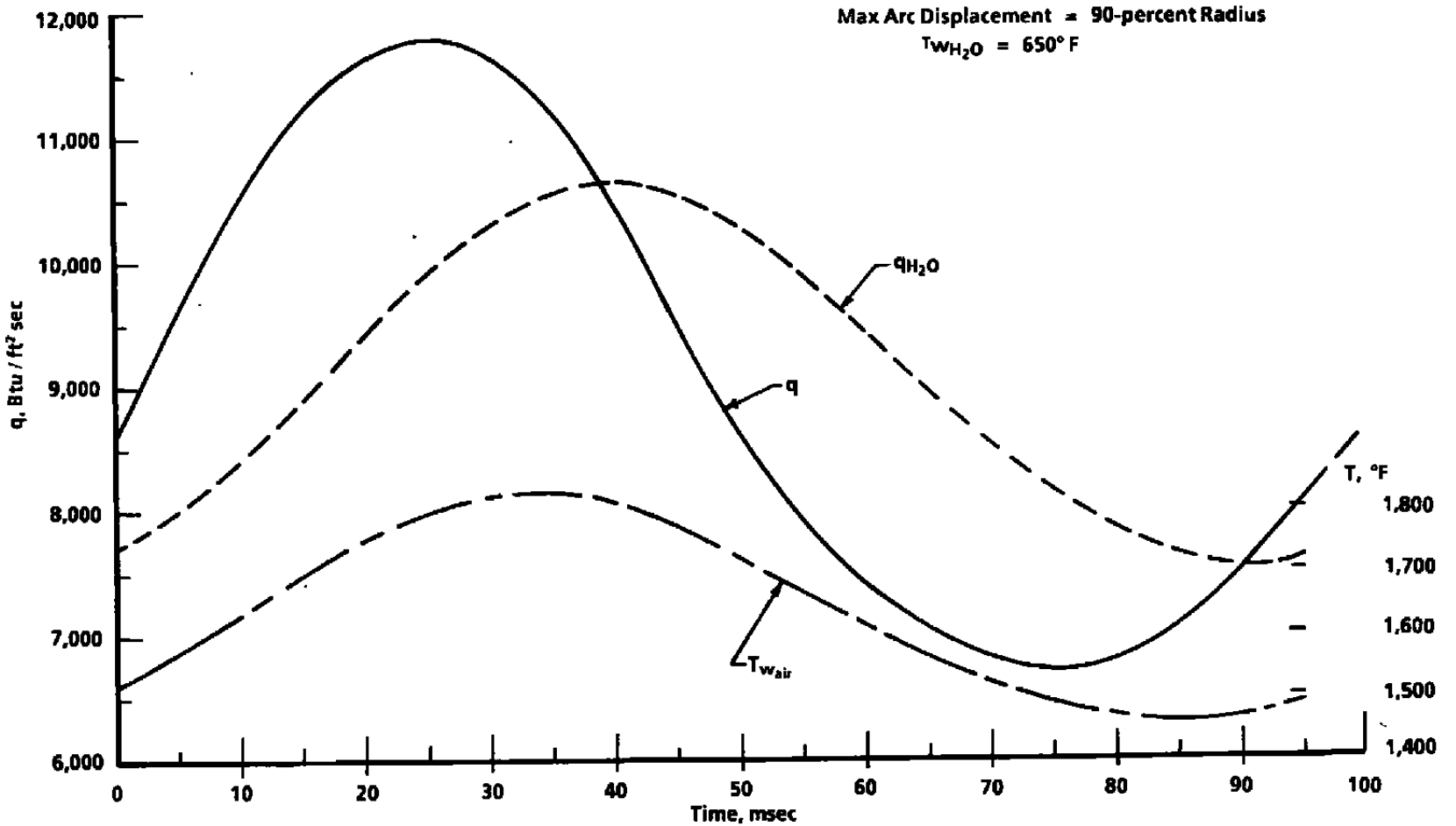

b. Period, λ = 0.1 sec

Figure 14. Concluded.

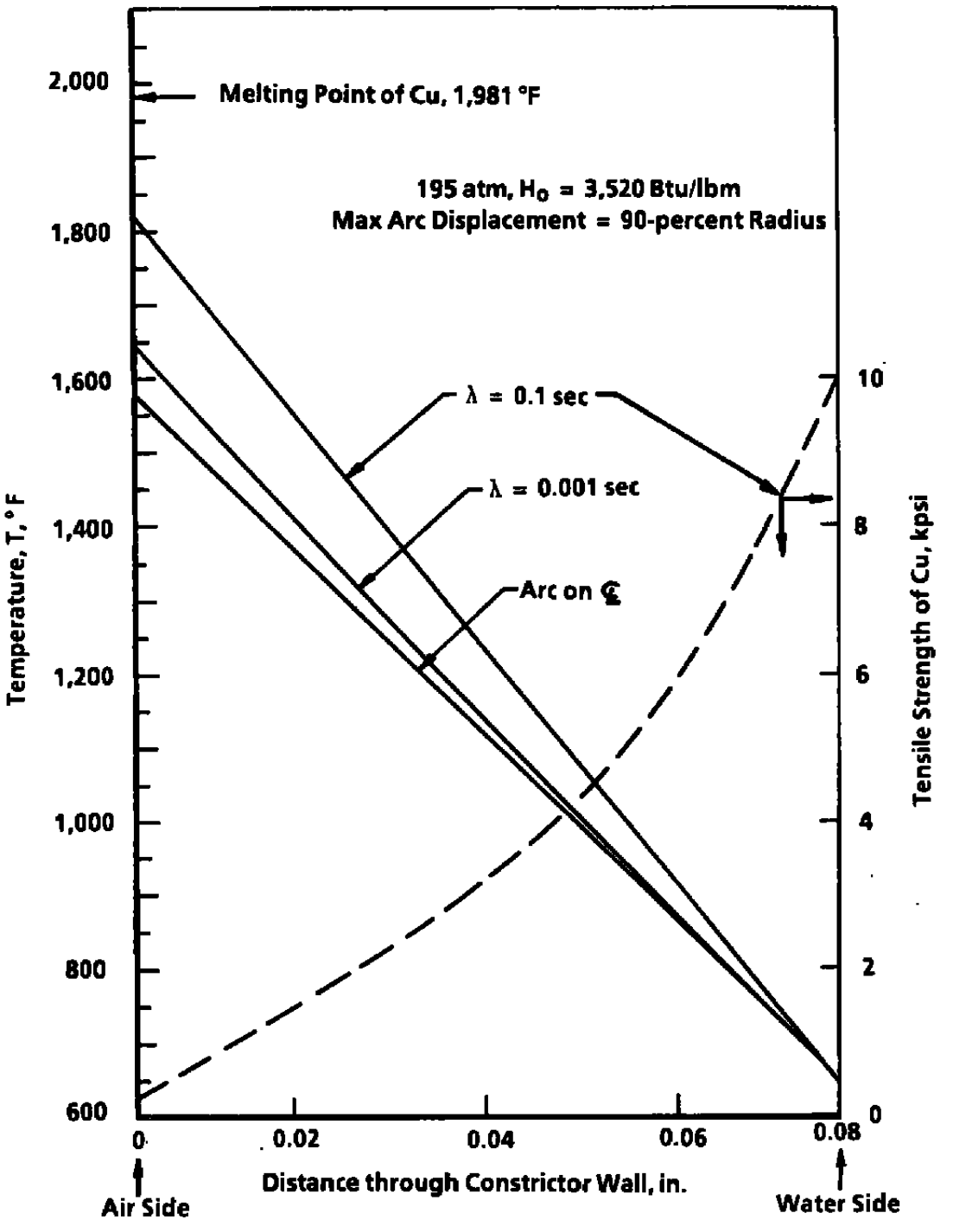

Figure 15. Predicted temperature and strength profiles in constrictor wall at maximum wall temperature.

$I_{IND} = B_T(1 - e^{-K_L X})$; $B_T = \sigma T^4/\pi$, K_L = Abs. Coefficient, 10.5 ev Band

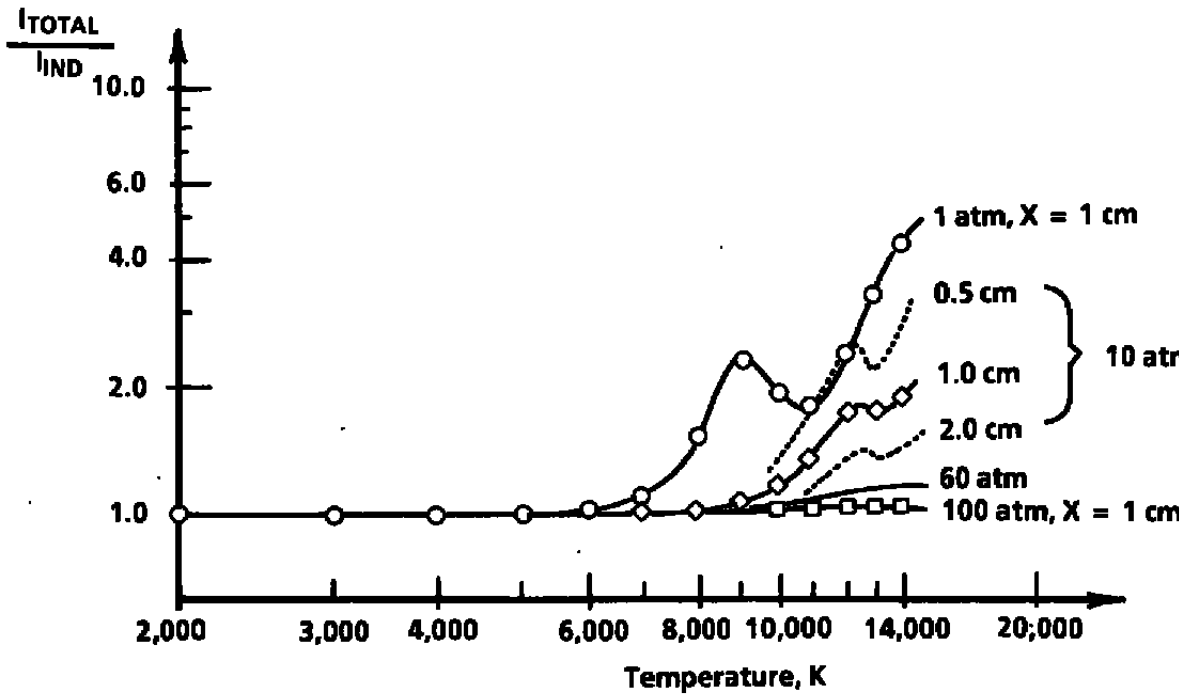

Figure 16. Ratio of total intensity to indicated intensity versus temperature (air).

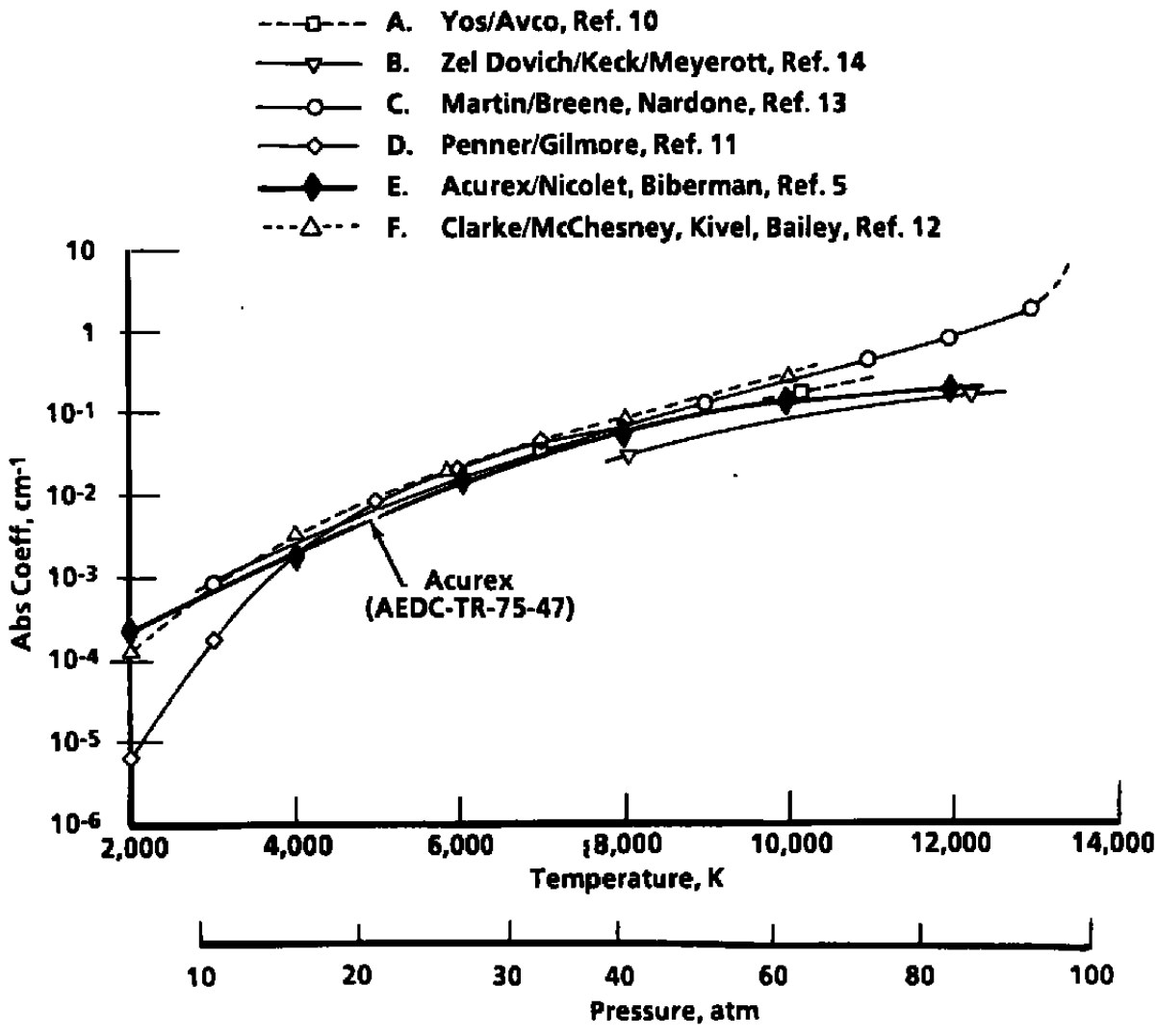

a. $\varrho/\varrho_0 = 1.0$ ($E_{photon} = 0 - 10.5$ ev)

Figure 17. Absorption coefficient of air versus temperature and density.

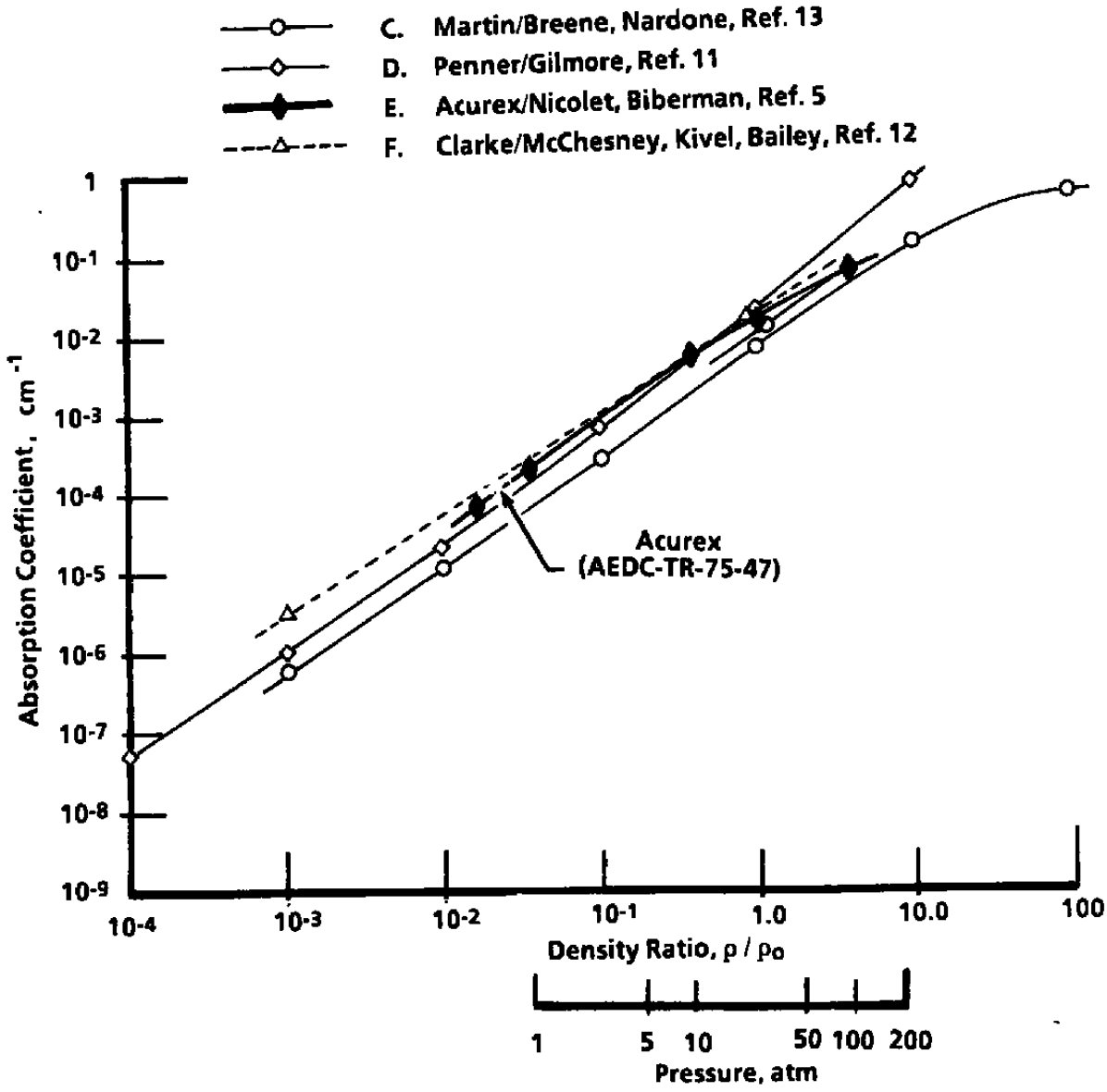

b. T = 6,000 K, E_{photon} = 0 – 10.5 ev

Figure 17. Concluded.

APPENDIX A

SOLUTION OF RADIANT ENERGY FIELD BY SPHERICAL HARMONIC FUNCTIONS

1.0 INFINITE SERIES EXPANSION

As described in Ref. 7, any arbitrary radiation field may be exactly specified by an infinite series of spherical harmonic functions. In three dimensions, the radiative transfer equation (Eq. 3) is:

$$\bar{\ell} \cdot \nabla I = -K \left[I - \frac{\sigma T^4}{\pi} \right] \tag{A-1}$$

where $\bar{\ell}$ is a unit vector in the direction of propagation and I is the frequency-integrated radiant intensity, Eq. (2). It is assumed that a general solution to Eq. (A-1) can be represented by an infinite series:

$$I(\bar{r}, \bar{\ell}) = \sum_{l=0}^{\infty} \sum_{m=-l}^{+l} A_l^m(\bar{r})\, Y_l^m(\bar{\ell}) \tag{A-2}$$

where $Y_l^m(\bar{\ell})$ are the spherical harmonic functions of direction and $A_l^m(\bar{r})$ are spatially dependent coefficients to be determined by boundary conditions on the radiation field.

By a standard procedure outlined in Ref. 7, the series Eq. (A-2) is substituted in the RTE, Eq. (A-1), followed by multiplication by the complex conjugate of Y_l^m, integration over 4π solid angle, and imposition of orthogonality and recurrence relations. A set of partial differential equations is obtained having the form:

$$\sum_{a=1}^{6} f_a(l,m)\, g_a \left(\frac{\partial A_{l\pm1}^{m\pm1}}{\partial x_{1,3}}, \frac{\partial A_{l\pm1}^{m}}{\partial x_2} \right) = -K \left[A_l^m + \frac{\sigma T^4}{\pi} \delta_{om} \delta_{ol} \right] \tag{A-3}$$

There is one such equation for each pair of the l and m indices. The δ's are Kronecker deltas and the x_i are Cartesian coordinates related to r, θ, ϕ, spherical coordinates by the direction cosines of the unit propagation vector, $\bar{\ell}$:

$$\ell_1 = x_1/r = \sin\theta \sin\phi;\ \ell_2 = x_2/r = \cos\theta;\ \ell_3 = x_3/r = \sin\theta \cos\phi \tag{A-4}$$

In the limit, as $l \to \infty$, this infinite set of simultaneous partial differential equations is completely equivalent to the integro-differential equations of the exact solutions. An N^{th} approximation to this system is obtained by terminating the series representation for the intensity function I **after the** $l = N^{th}$ term. There will always be $(N + 1)^2$ equations of the

intensity function I after the l = Nth term. There will always be $(N + 1)^2$ equations of the type of Eq. (A-3) involving the same number of A_l^m coefficients. As N increases, the system of equations becomes a closer and closer approximation to the infinite set. It is known from neutron transport theory that the first approximation (N = 1) is sufficiently accurate for many radiation fields; that is:

$$I(\bar{r}, \bar{\ell}) = A_0^0 Y_0^0 + A_1^{-1} Y_1^{-1} + A_1^0 Y_1^0 + A_1^1 Y_1^1 + \ldots \tag{A-5}$$

The four equations of type Eq. (A-3) in this approximation could be solved directly for the four A_l^m coefficients, thus defining the radiation field intensity for given boundary conditions. Instead, however, advantage is taken of the fact that the space-integrated intensity

$$I_o = \int_0^{4\pi} I(\bar{r}, \bar{\ell})\, d\Omega \tag{A-6}$$

and the radiant flux vector $\bar{q}^R$ are also functions of the four A_l^m coefficients, so that in combination with the four partial differential equations of type Eq. (A-3), the following two relations are developed:

$$\frac{\partial q_1}{\partial x_1} + \frac{\partial q_2}{\partial x_2} + \frac{\partial q_3}{\partial x_3} = -K\left[I_o - 4\sigma T^4\right] \tag{A-7}$$

$$\frac{\partial I_0}{\partial x_1}\bar{i}_1 + \frac{\partial I_o}{\partial x_2}\bar{i}_2 + \frac{\partial I_0}{\partial x_3}\bar{i}_3 = -3K\left[q_1\bar{i}_1 + q_2\bar{i}_2 + q_3\bar{i}_3\right] \tag{A-8}$$

In vector notation, finally,

$$\nabla \cdot \bar{q}^R = -K\left[I_o - 4\sigma T^4\right] \tag{A-9}$$

$$\nabla I_o = -3K\,\bar{q}^R \tag{A-10}$$

Equations (A-9) and (A-10) are identical to the relations which are obtained by moment methods and also referred to as the diffusion or differential approximations (Sec. 4.1).

If the appropriate spherical harmonic functions (Ref. 7) are substituted in Eq. (A-5), the radiation intensity in this approximation can be expressed as

$$I(\bar{r},\bar{\ell}) = \frac{1}{4\pi}\left(I_o(\bar{r}) + 3\,\bar{q}^R \cdot \bar{\ell}\right) \tag{A-11}$$

for general radiation fields, and

$$I(\bar{r}, \bar{\ell}) = \frac{1}{4\pi}\left(I_o(\bar{r}) + 3\,q\cos\theta\right) \tag{A-12}$$

for simple planar radiation fields in which θ is the angle between direction of propagation and the heat flux vector $\bar{q}^R$. The intensity is thus the spatial average value $I_o/4\pi$ plus a directionally dependent contribution related to the heat flux.

2.0 BOUNDARY CONDITIONS

The boundary condition associated with the exact radiative transfer Eq. (A-1) is simply that the outward radiant intensity at a black wall is equal to the blackbody intensity of the wall temperature, uniform in all directions:

$$I^+ \left(\bar{r}, \bar{\ell}\right) = \frac{\sigma T_w^4}{\pi}, \quad \bar{\ell} \cdot \bar{n} \geq 0 \tag{A-13}$$

If the RTE is properly integrated with respect to distance from this wall value over all possible directions, with a known gas temperature distribution, the exact solution for I ($\bar{r}$, $\bar{\ell}$) is uniquely determined. If the spherical harmonic expansion of the radiation field is used, on the other hand, this boundary condition is replaced by an infinite set of boundary conditions obtained by substitution of the series expansion for intensity Eq. (A-2) in (A-13). In the limit of $l \rightarrow \infty$, this set of boundary conditions combined with Eq. (A-3) is entirely equivalent to the combination of Eqs. (A-1) and (A-13).

In any finite-order approximation of spherical harmonics, however, the exact boundary condition cannot be met because a truncated series for I, such as Eq. (A-5), cannot represent a directionally independent intensity at a wall, except for the case of zero radiant heat flux. An approximation to the boundary condition, Eq. (A-13), must be adopted and, moreover, many different approximations are possible. The most frequently used boundary condition approximations are those developed in neutron transport theory for problems with planar geometry and dependence upon a single space coordinate (Ref. 7):

1. Mark's boundary condition simply requires that the radiant intensity, $I = 1/4\pi \times (I_o + 3\, q \cos\theta)$, at the wall be equal to the blackbody intensity only in a single discrete direction given by $\theta_i = \cos^{-1}(1\ \sqrt{3}) = 54.7°$.

2. Marshak's boundary condition requires an intensity distribution at the wall which produces an integrated radiant heat flux from the wall equal to that of a blackbody.

These two approximate boundary conditions then relate integrated intensity I_o, heat flux q, and wall temperature by

$$\left[I_o + mq\right]_{wall} = 4\sigma T_w^4 \tag{A-14}$$

with $m = \sqrt{3}$ for the Mark condition and $m = 2.0$ for the Marshak condition.

Reference 7 states that extension of this relation to more general radiation fields is neither straightforward nor free of ambiguities. On the other hand, the three-dimensional field associated with a variable-temperature plane wall has a first-order Marshak boundary condition which is cited as:

$$I_o\,(x_1, 0, x_3) + 2q_2\,(x_1, 0, x_3) = 4\sigma T_w^4\,(x_1, 0, x_3) \qquad \text{(A-15)}$$

only marginally different from Eq. (A-14). Based on this similarity, it is assumed that boundary conditions for other nonplanar fields such as those occurring in arc heaters may be obtained from Eq. (A-14) without serious error.

3.0 THE DIFFUSION APPROXIMATION

The approximate solution to the problem of radiant transport of energy, Eqs. (A-9) and (A-10) with appropriate boundary conditions, is often referred to as the "diffusion" approximation. This is based on the similarity of Eq. (A-10) to the relation for molecular diffusion of neutral particles:

$$q_{diff} = -D\frac{dn}{dx} = -\frac{L\bar{c}}{3}\frac{dn}{dx} \qquad \text{(A-16)}$$

where q_{diff} is the molecular number flux, D is the binary diffusion coefficient, L is the mean free path, $\bar{c}$ is mean molecular speed, and dn/dx is the concentration gradient. The analogy is made apparent by converting Eq. (A-10) to a photon flux:

$$\text{photon flux} = \frac{\bar{q}}{h\nu} = -\frac{1}{3Kh\nu}\nabla\left(n_p h\nu c\right) = \frac{-c}{3K}\nabla\left(n_p\right) \qquad \text{(A-17)}$$

where c is the speed of light. The absorption coefficient, K, is thus identified as the reciprocal of a mean free path in absorption.

NOMENCLATURE

a,b	Constants, Eq. (14)
A,Y	Coefficients, Eq. (A-2)
B	Blackbody intensity
c	Mean molecular speed or speed of light
D	Binary diffusion coefficient
D_n,E_n	Exponential integral functions, Eqs. (11) and (16)
D_1,D_2,D_3	Exponential functions, Eq. (17)
E_1,E_2,E_3	Exponential functions, Eq. (14)
h	Planck's constant
H	Enthalpy
i	Unit vector
I	Frequency-integrated radiant intensity or current
I_ν	Spectral radiant intensity function
I_o	Space integrated radiant intensity
K	Absorption coefficient
ℓ	Direction cosine
$\bar{\ell}$	Unit vector in direction of propagation
L	Mean free path
m	Constant, Eq. (A-14)

n	Direction normal to surface or particle density
P	Pressure
q	Heat flux
$\bar{r}$	Position vector
r,θ,ϕ	Spherical coordinates
S	Distance in direction of propagation
T	Temperature
W	Band weight factor
X,Y,Z	Cartesian coordinates
δ	Kronecker delta
η	Optical thickness, Eq. (9)
ν	Frequency
σ	Stefan-Boltzman constant
τ	Optical depth, Eq. (5)
Ω	Solid angle
Δ	Thickness (distance between plane walls)
λ	Period, sec

Subscripts

B	Boundary
H	High-energy band

i	Coordinate indices 1, 2, 3
L	Left or low-energy band
o	Standard temperature/pressure
p	Photon
R	Right
S	Position along direction of propagation
W	Wall
ν	Photon frequency

Superscripts

R	Radiation
'	Dummy variable of integration